ELSEVIER

International Journal of Solids and Structures 41 (2004) 2011–2037

INTERNATIONAL JOURNAL OF SOLIDS and STRUCTURES

www.elsevier.com/locate/ijsolstr

Deformation process design for control of microstructure in the presence of dynamic recrystallization and grain growth mechanisms

Shankar Ganapathysubramanian, Nicholas Zabaras *

Materials Process Design and Control Laboratory, Sibley School of Mechanical and Aerospace Engineering, Cornell University, 188 Frank H.T. Rhodes Hall, Ithaca, NY 14853-3801, USA

Received 12 December 2002; received in revised form 20 October 2003

Abstract

The idea of control of mechanical properties in materials through designer processing techniques is promoted through this effort, in contrast to the standard control by alloying. Microstructure evolution through dynamic recrystallization is accurately modelled for the large thermo-mechanical deformation of hyperelastic thermo-viscoplastic materials. An innovative solution strategy and a computational algorithm are presented for the solution of the direct deformation problem comprised of the kinematic, constitutive, contact and thermal sub-problems. The description relies on microstructure based scalar state variables. The formulation follows an approach introduced earlier by Busso [International Journal of Plasticity 14(4–5) (1998) 319] that considers an instability criterion to define the onset of recrystallization. The analysis is performed for hot forming processes and the kinetics of grain growth is controlled by the grain boundary energies and the energy stored through the dislocation density. A finite element implementation is presented and validated with available numerical and experimental results.

In addition, an innovative computational framework is developed for the design of deformation processes using the continuum sensitivity method (CSM) incorporating microstructure related state variables. This CSM involves considering the direct continuum equations, design-differentiating them and then evaluating their discretized form. This method differs from common sensitivity techniques in which one design-differentiates the direct discretized equations. The developed method is validated by comparing the computed sensitivities to those obtained through a finite difference scheme. In addition, a gradient-based optimization framework is developed which uses the continuum sensitivity method to evaluate the gradients of the objective functions and constraints. The effectiveness of the method is demonstrated through a number of applications in the design optimization of hot forming processes in the presence of recrystallization and grain growth mechanisms. These examples cover a wide range of applications as they include parameter design (e.g., die design), preform design as well as multi-stage forming design.

Keywords: Continuum sensitivity analysis; Dynamic recrystallization; Metal forming; Elasto-plasticity; Thermo-mechanical analysis; Optimization; Computational design

* Corresponding author. Tel.: +1-607-255-9104; fax: +1-607-255-9410.
E-mail address: zabaras@cornell.edu (N. Zabaras).

0020-7683/$ - see front matter © 2003 Elsevier Ltd. All rights reserved.
doi:10.1016/j.ijsolstr.2003.11.020

1. Introduction

It is well understood that the properties of a metal are strongly influenced by its microstructural features like the grain size and the grain/sub-grain orientation/mis-orientation. During thermo-mechanical deformation processes, materials experience significant microstructural changes which in turn strongly affect their mechanical properties. The mechanisms of microstructure evolution during thermo-mechanical processing include strain hardening, recrystallization and grain growth. The main reason for this renewed interest lies in the attractiveness of control of microstructural properties in metallic materials by processing rather than by alloying—the current, expensive industrial practice.

There have been extensive efforts, over the years, to understand the physics behind the evolution of microstructure. The stored energy was established early as one of the important driving forces behind recrystallization. Following this, many parameters affecting the process of recrystallization were identified. In a crystalline solid, the free energy of the material is increased during deformation by the presence of dislocations. On annealing however, the microstructure and the properties may be partially restored to the original values by the process of recovery that involves only a partial restoration as the material reaches a meta-stable state. Recrystallization is a further restoration process wherein new dislocation free grains are formed within the deformed microstructure. Recrystallization may also take place during deformation at elevated temperatures and this is termed as dynamic recrystallization. Our emphasis here is primarily with modelling and control of dynamic recrystallization occurring in metals during hot forming operations. Recrystallization removes most of the dislocations, but the material still contains grain/sub-grain boundaries, which are thermodynamically unstable. Furthermore, grain growth results in the elimination of small grains, the growth of larger grains (both recrystallized and not recrystallized grains) and the grain boundaries assuming a configuration of minimum energy. As normally the recrystallized grains are smaller than the non-recrystallized grains, grain growth essentially leads to the growth of non-recrystallized grains. This growth of grains is further classified into normal and abnormal grain growth depending upon the kinetics of the process. In this effort, we constrain ourselves to normal grain growth. The main parameters which have been identified to affect recrystallization include kinetics, straining rates and temperature. The key literature, which describes recrystallization, affecting parameters and methods of control include Cotterill and Mould (1976) and Humphreys and Hatherly (1995). An effort towards the development of a continuum theory for dynamic recrystallization involves the work by Busso (1998), where a hypoelastic constitutive framework is used.

Some work has also been performed on the control of microstructure in deformation processes that include dynamic recrystallization. One recent effort towards design of deformation processes for uniform microstructure is described in Lee et al. (2000). Here, the design of the die profile is carried out to yield uniform microstructure (i.e., obtain uniform grain size distribution) in a hot extruded product. The analysis is based on Yada and Senuma's empirical equations for recrystallization and grain growth (Yada and Senuma, 1986) and it involves a rigid, thermo-viscoplastic finite element analysis and considers both static and dynamic recrystallization. Gao and Grandhi (2000) have also analyzed the problem of microstructure optimization during hot forming processes. In their effort, a direct differentiation scheme is employed for evaluating the sensitivities for a material (Waspaloy) undergoing dynamic recrystallization. Malas et al. (1997) studied the control of microstructure during hot working processes based on optimal control theory and developed state-space models for describing the material response as well as the mechanics of the process. This method was then applied to the optimization of grain size and process parameters by appropriately defining the die geometry and ram velocity during the steady extrusion of plain carbon steel.

This work is expanding our existing capabilities in deformation process design (Ganapathysubramanian and Zabaras, 2002, 2003) to account for dynamic recrystallization and related grain growth processes. It provides a methodology to accurately model dynamic recrystallization (recrystallization during hot deformation process) by incorporating explicitly the various microstructural length scales that describe the

state of the evolving microstructure. Our work follows that of Busso (1998) and incorporates an instability (localization) criterion for the onset of recrystallization. A hyperelastic–viscoplastic framework is adopted and a fully implicit radial-return mapping is considered for the integration of the constitutive model. This is described in Section 2. The kinetics of recrystallization are provided in great detail in Section 2.2.

A continuum sensitivity problem is then introduced and a novel computational scheme for evaluating the sensitivity fields is presented. One of the more attractive features of this model is the sensitivity problem, which follows a design-differentiate and then discretize approach, rather than the standard, discretize and then design-differentiate approach. The sensitivity analysis, which involves the kinematic, constitutive, contact and thermal sensitivity sub-problems is presented in Section 3. The computed sensitivities are validated and used in a gradient based optimization framework for the control of microstructure during deformation processes. To our knowledge, this is the first time that a rigorous sensitivity framework is presented for deformation process design that accounts for dynamic recrystallization and grain growth mechanisms.

2. Direct deformation problem

The direct problem can be stated as follows: Compute the time history of deformation, temperature and material state of a body deforming as a result of external forces and/or deformation due to contact and friction at the workpiece–die interface. This deformation problem, which involves coupled mechanical and thermal effects, is sub-divided into kinematic, constitutive, contact and thermal sub-problems. We shall only provide a brief outline of the solution strategy as this direct problem is described extensively in our earlier publications (Srikanth and Zabaras, 1999a).

2.1. Problem description

Consider $\mathscr{B}_0$ as the initial configuration of the body (at time $t = 0$) and $\mathscr{B}_{n+1}$ as the current configuration. The reference configuration $\mathscr{B}_{\mathrm{r}}$ is taken as $\mathscr{B}_0$ in the total Lagrangian formulation and $\mathscr{B}_n$ in an updated Lagrangian formulation. The total deformation gradient is then defined as follows in a total Lagrangian framework:

$$\boldsymbol{F}(\boldsymbol{X},t) = \nabla_0 \phi(\boldsymbol{X},t) = \frac{\partial \phi(\boldsymbol{X},t)}{\partial \boldsymbol{X}}, \quad \det \boldsymbol{F} > 0 \tag{2.1}$$

where $\phi(\boldsymbol{X},t)$ represents the deformation map from $\mathscr{B}_0$ to $\mathscr{B}_{n+1}$. Using an updated Lagrangian framework, one can introduce the relative deformation gradient $\boldsymbol{F}_{\mathrm{r}}$ and express $\boldsymbol{F}_{n+1}$ as shown below:

$$\boldsymbol{F}_{n+1} = \nabla_0 \phi(\boldsymbol{X}, t_{n+1}) = \nabla_n \tilde{\phi}(\boldsymbol{x}_n, t_{n+1}) \nabla_0 \phi(\boldsymbol{X}, t_n) = \boldsymbol{F}_{\mathrm{r}} \boldsymbol{F}_n \tag{2.2}$$

In the above and all following equations, the subscript $n+1$ will be omitted for all fields defined in the current configuration and the subscript r will be used to indicate the reference configuration $\mathscr{B}_n$ in an updated Lagrangian framework. In an appropriate kinematic framework for large deformation inelastic analysis incorporating thermal effects, the total deformation gradient is decomposed into thermal, plastic and elastic parts as follows:

$$\boldsymbol{F} = \boldsymbol{F}^{\mathrm{e}} \boldsymbol{F}^{\mathrm{p}} \boldsymbol{F}^{\theta} \tag{2.3}$$

where $\boldsymbol{F}^{\mathrm{e}}$ is the elastic deformation gradient, $\boldsymbol{F}^{\mathrm{p}}$, the plastic deformation gradient and $\boldsymbol{F}^{\theta}$ is the thermal part of the deformation gradient.

With the above kinematic framework, notions of an intermediate thermally expanded hot unstressed configuration and that of an intermediate hot plastically deformed relaxed configuration are introduced.

Assuming isotropic thermal expansion, the evolution of the intermediate thermally expanded unstressed configuration is given as follows:

$$\dot{\boldsymbol{F}}^{\theta}(\boldsymbol{F}^{\theta})^{-1} = \beta\dot{\theta}\boldsymbol{I} \tag{2.4}$$

where β is the thermal expansion coefficient, treated as a constant in this work and $\boldsymbol{I}$ is the second-order identity tensor.

Following the work of Anand (Brown et al., 1989; Anand, 1985), the hyper-elastic constitutive equation is written as

$$\overline{\boldsymbol{T}} = \mathscr{L}^{\mathrm{e}}[\overline{\boldsymbol{E}}^{\mathrm{e}}] \tag{2.5}$$

where the strain measure, $\overline{\boldsymbol{E}}^{\mathrm{e}}$, is defined with respect to the intermediate (unstressed) configuration as $\overline{\boldsymbol{E}}^{\mathrm{e}} = \ln \boldsymbol{U}^{\mathrm{e}}$. The corresponding conjugate stress measure $\overline{\boldsymbol{T}}$ is the pullback of the Kirchhoff stress with respect to $\boldsymbol{R}^{\mathrm{e}}$,

$$\overline{\boldsymbol{T}} = \det(\boldsymbol{U}^{\mathrm{e}})(\boldsymbol{R}^{\mathrm{e}})^{\mathrm{T}}\boldsymbol{T}\boldsymbol{R}^{\mathrm{e}} \tag{2.6}$$

Here $\boldsymbol{U}^{\mathrm{e}}$ and $\boldsymbol{R}^{\mathrm{e}}$ are calculated from the polar decomposition, $\boldsymbol{F}^{\mathrm{e}} = \boldsymbol{R}^{\mathrm{e}}\boldsymbol{U}^{\mathrm{e}}$, of $\boldsymbol{F}^{\mathrm{e}}$. For an isotropic material, the elastic moduli $\mathscr{L}^{\mathrm{e}}$ is given by

$$\mathscr{L}^{\mathrm{e}} = 2\mu\mathscr{I} + \left\{\kappa - \tfrac{2}{3}\mu\right\}\boldsymbol{I}\otimes\boldsymbol{I} \tag{2.7}$$

where μ is the shear modulus, κ is the bulk modulus and $\mathscr{I}$ denotes the fourth order identity tensor.

The evolution of $\boldsymbol{F}^{\mathrm{p}}$ is modelled using the classical J_2 theory with one scalar state variable s which represents the isotropic hardening material behavior. The evolution of the plastic deformation gradient $\boldsymbol{F}^{\mathrm{p}}$ is given by the normality rule,

$$\overline{\boldsymbol{L}}^{\mathrm{p}} = \dot{\boldsymbol{F}}^{\mathrm{p}}(\boldsymbol{F}^{\mathrm{p}})^{-1} \tag{2.8}$$

where $\overline{\boldsymbol{L}}^{\mathrm{p}} = \overline{\boldsymbol{D}}^{\mathrm{p}}$ and $\overline{\boldsymbol{W}}^{\mathrm{p}} = \boldsymbol{0}$.

The flow rule can be stated as

$$\overline{\boldsymbol{D}}^{\mathrm{p}} = \sqrt{\frac{3}{2}}\dot{\tilde{\epsilon}}^{\mathrm{p}}\frac{\overline{\boldsymbol{T}}'}{\|\overline{\boldsymbol{T}}'\|} \tag{2.9}$$

where $\tilde{\epsilon}$ is the equivalent strain rate to be defined in Section 2.2.

The equilibrium equation can be expressed on the reference configuration as

$$\nabla_{\mathrm{r}}\cdot\boldsymbol{P}_{\mathrm{r}} + \boldsymbol{f} = \boldsymbol{0} \tag{2.10}$$

where $\nabla_{\mathrm{r}}\cdot$ represents the divergence in the reference configuration. The Piola–Kirchhoff I stress, $\boldsymbol{P}_{\mathrm{r}}$ is expressed as

$$\boldsymbol{P}_{\mathrm{r}} = \det\boldsymbol{F}_{\mathrm{r}}\boldsymbol{T}\boldsymbol{F}_{\mathrm{r}}^{-\mathrm{T}} \tag{2.11}$$

Recall that for the total Lagrangian analysis, $\boldsymbol{F}_{\mathrm{r}} = \boldsymbol{F}$.

The solution of the deformation problem proceeds incrementally in time starting from the initial configuration $\mathscr{B}_0$. In order to solve the equilibrium equations at time $t = t_{n+1}$, the constitutive relationship between the Cauchy stress $\boldsymbol{T}$ and the set involving the relative deformation gradient $\boldsymbol{F}_{\mathrm{r}}$ and temperature θ should be evaluated. This is shown in Srikanth and Zabaras (1999a).

2.2. Constitutive problem

Microstructure related length scales are now introduced into the constitutive framework to model the dependence of the material behavior on its recrystallized state. We describe the microstructure through internal state variables linked to the grain size as followed by Busso (1998) and Dunne et al. (1997). The evolution of the equivalent tensile plastic strain is specified via the following functional form:

$$\dot{\bar{\epsilon}}^{\mathrm{p}} = f\left(\tilde{\sigma}, s, \theta, \frac{L_0}{L}\right) \tag{2.12}$$

where L_0 is the initial mean grain size, $\tilde{\sigma}$ is the equivalent stress, s is the state variable denoting the deformation resistance, θ is the absolute temperature and L denotes the mean grain size. Before we proceed with the detailed analysis of the constitutive model, we describe, for clarity, some of the terms to be used in the following text. As discussed earlier, emphasis is here given to grain refinement and growth during dynamic recrystallization in materials. We herein define primary recrystallization as the region of recrystallization that mostly involves grain refinement and secondary recrystallization as that region which involves grain growth. Prior to the onset of primary recrystallization, we assume $L = L_0$ and hence Eq. (2.12) reduces to the form where strain rate sensitivity is independent of grain size.

The evolution of the isotropic scalar resistance s is assumed to take the form:

$$\dot{s} = g(\tilde{\sigma}, s, \theta, L) = h(\tilde{\sigma}, s, \theta, L) - \dot{r}(\tilde{\sigma}, s, \theta, L) \tag{2.13}$$

where $\dot{r}(\tilde{\sigma}, s, \theta, L)$ is a dynamic recovery function (recovery during deformation) associated with recrystallization, which describes the annihilation rate of dislocations and is responsible for the nucleation of new grains. The function $h(\tilde{\sigma}, s, \theta, L)$ is associated with deformation processes and is interpreted as the rate at which the average dislocation density evolves (increases/decreases) in the material.

2.2.1. Hardening law

The hardening rate is defined as follows:

$$h(\tilde{\sigma}, s, \theta, L) = \hat{h}(s, s^*, \tilde{\sigma}, \theta, L, L_0) \tag{2.14}$$

where s^* represents a saturated or steady state condition. This law also needs to allow for strain softening due to a sudden increase in local temperature. A functional dependence of s^* consistent with the behavior that a decrease in mean grain size causes the steady state dislocation density and hence s^* to decrease is the following:

$$s^* = s^*\left(\frac{L}{L_0}, \dot{\bar{\epsilon}}^{\mathrm{p}}, \theta\right) \tag{2.15}$$

Experimental evidence suggest that the time scale associated with primary recrystallization is much smaller than that required to reach a stable dynamic state. This dynamic balance is a concept implicit to our analysis of the evolution of the deformation resistance. We assume that the deformation resistance reaches a saturation state and this occurs only if there exists a dynamically stable state between grain refinement and growth. We then let L^* be the mean grain size when such a dynamically balanced state exists, then the above equation can be modified, accounting for the above mentioned time scale effect as follows:

$$s^* = s^*\left(\frac{L^*}{L_0}, \dot{\bar{\epsilon}}^{\mathrm{p}}, \theta\right) \tag{2.16}$$

2.2.2. Dynamic recrystallization recovery law

The driving force for recrystallization is known to be supplied by the stored energy towards the nucleation of new grains both within the interior of the grain and at the grain boundaries. A general form of

the dynamic recrystallization recovery function with this driving force given in terms of the deformation resistance, $s - s_f$, is the following:

$$\dot{r}(\tilde{\sigma}, s, \theta, L) = f_R \widehat{X}_R(\tilde{\sigma}, s, L, \theta)(s - s_f)\dot{\tilde{\epsilon}}^{\mathrm{p}} \tag{2.17}$$

where f_R is a material parameter which defines the magnitude of recovery, s_f is the deformation resistance at the end of primary recrystallization and the function $\widehat{X}_R$ represents the volume fraction of the recrystallized material associated with the current state (s, L). Expression for $\widehat{X}_R$ can be motivated by the classical treatment of the kinetics of grain growth, as is done in this effort. We further denote, for convenience, $\widehat{X}_R(\tilde{\sigma}, s, L, \theta)$ by X_R.

2.2.3. Kinetics of grain growth

The evolution of the average grain size during and immediately after primary recrystallization (during dynamic recrystallization) is considered to be governed by the following equation:

$$\dot{L} = l(\tilde{\sigma}, s, L, \theta) = \dot{L}_{\mathrm{ref}} + \dot{L}_{\mathrm{grow}} \tag{2.18}$$

where $\dot{L}_{\mathrm{ref}}$ is a function that describes the overall grain refinement taking place during primary recrystallization and $\dot{L}_{\mathrm{grow}}$ represents the kinetics of grain growth process driven by grain boundary energies during secondary recrystallization. $\dot{L}_{\mathrm{ref}}$ is driven by the dynamic imbalance between nucleation and grain growth events, $(L - L^*)$, and is given as follows:

$$\dot{L}_{\mathrm{ref}} = -f_R X_R \prec L - L^* \succ \dot{\tilde{\epsilon}}^{\mathrm{p}} \tag{2.19}$$

where f_R is a material constant and $\prec x \succ$ denote x if $x \geqslant 0$ and 0 if $x < 0$.

Grain growth is now characterized by the following equation:

$$\dot{L}_{\mathrm{grow}} = \dot{L}_0(1 - \exp(- \prec X_R - X_{Rc} \succ)) \exp\left(-\frac{\mathcal{Q}}{R\theta}\right)\left(\frac{L_0}{L}\right) \tag{2.20}$$

where $\dot{L}_0$ is a material constant, the Arrhenius and inverse terms account for the increase in grain boundary mobility for increasing temperatures and decreasing mean grain sizes, and X_{Rc} is the volume fraction recrystallized at the end of primary recrystallization (i.e., the end of the refinement process).

Recrystallization can be treated as a localization phenomena and the critical strain for the onset of recrystallization is given by

$$\tilde{\epsilon}^{\mathrm{p}}_C = \frac{2}{\sqrt{3}} \frac{C_{\mathrm{c}}}{\mu}(f_C s^* - s_0) \tag{2.21}$$

and $\tilde{\epsilon}^{\mathrm{p}}_R$, the strain needed to complete strain softening and leaving the material in partially recrystallized state, is given by

$$\tilde{\epsilon}^{\mathrm{p}}_R = \frac{2}{\sqrt{3}} \frac{C_R}{\mu} s_0^* f_1(L, L^*) \tag{2.22}$$

where C_{c}, C_R, f_C are material parameters and f_1 is a function measuring the dynamic imbalance.

2.3. Time integration of the constitutive problem

A brief review is presented here of the radial return algorithm implemented for the integration of the constitutive problem. In the incremental constitutive problem, one evaluates the set $(\overline{\boldsymbol{T}}_{n+1}, s_{n+1}, L_{n+1}, \boldsymbol{F}^{\mathrm{p}}_{n+1})$, with the body configurations at time t_n, t_{n+1} and the set $(\overline{\boldsymbol{T}}_n, s_n, L_n, \boldsymbol{F}^{\mathrm{p}}_n, \theta_{n+1})$ known. Considering a backward Euler technique for the time integration of Eqs. (2.8), (2.13) and (2.18), one can obtain the following:

$$\boldsymbol{F}^{\mathrm{p}}_{n+1} = \exp(\Delta t \overline{\boldsymbol{D}}^{\mathrm{p}}_{n+1}) \boldsymbol{F}^{\mathrm{p}}_{n} \tag{2.23}$$

$$s_{n+1} = s_n + \Delta t g(\tilde{\sigma}_{n+1}, s_{n+1}, \theta_{n+1}, L_{n+1}) \tag{2.24}$$

and

$$L_{n+1} = L_n + \Delta t l(\tilde{\sigma}_{n+1}, s_{n+1}, \theta_{n+1}, L_{n+1}) \tag{2.25}$$

We introduce a trial elastic deformation gradient, $\boldsymbol{F}^{\mathrm{e}}_{*}$, defined as $\boldsymbol{F}^{\mathrm{e}}_{*} = \boldsymbol{F}_{\mathrm{r}} \boldsymbol{F}^{\mathrm{e}}_{n} = \boldsymbol{R}^{\mathrm{e}}_{*} \boldsymbol{U}^{\mathrm{e}}_{*}$, where $\boldsymbol{F}_{\mathrm{r}}$ has been defined earlier. We then define the trial stress as $\overline{\boldsymbol{T}}_{*} = \mathscr{L}^{\mathrm{e}}[\overline{\boldsymbol{E}}^{\mathrm{e}}_{*}]$. The equivalent trial stress is defined, from the deviatoric part of the trial stress, as follows:

$$\tilde{\sigma}_{*} = \sqrt{\tfrac{3}{2} \overline{\boldsymbol{T}}'_{*} \cdot \overline{\boldsymbol{T}}'_{*}} \tag{2.26}$$

and the pressure is defined as

$$p_{*} = -\tfrac{1}{3} \mathrm{tr}\, \overline{\boldsymbol{T}}_{*} \tag{2.27}$$

Following similar steps to the derivations in Weber and Anand (1990), it can be shown that $\overline{\boldsymbol{T}}'_{*}$ and $\overline{\boldsymbol{T}}'_{n+1}$ are in the same direction:

$$\overline{N}_{n+1} = \sqrt{\frac{3}{2}} \frac{\overline{\boldsymbol{T}}'_{*}}{\tilde{\sigma}_{*}} \tag{2.28}$$

Thus only the scalars, $\tilde{\sigma}_{n+1}$, s_{n+1}, p_{n+1} and L_{n+1} need be evaluated. It can further be shown that $p_{n+1} = p_{*}$ and that $\tilde{\sigma}_{n+1}$ is governed by the following scalar equation:

$$\tilde{\sigma}_{n+1} - \tilde{\sigma}_{*} + 3\Delta t \mu \dot{\tilde{\epsilon}}^{\mathrm{p}}(\tilde{\sigma}_{n+1}, s_{n+1}, \theta_{n+1}, L_{n+1}) = 0 \tag{2.29}$$

The evolution equations for the deformation resistance s_{n+1} and the mean grain size L_{n+1} along with the relation for the equivalent stress $\tilde{\sigma}_{n+1}$ (i.e., Eqs. (2.24), (2.25) and (2.29)), are solved simultaneously, within a time step, using a Newton–Raphson procedure incorporating a line search algorithm. This was found to be very efficient for material models considered in the examples to be discussed later.

With these values of parameters, we can update the Cauchy stress as follows:

$$\boldsymbol{T}_{n+1} = \exp\left(\frac{p_{*}}{\kappa}\right) \boldsymbol{R}^{\mathrm{e}}_{*} \overline{\boldsymbol{T}}_{n+1} (\boldsymbol{R}^{\mathrm{e}}_{*})^{\mathrm{T}} \tag{2.30}$$

with $\overline{\boldsymbol{T}}'_{n+1} = \eta_{n+1} \overline{\boldsymbol{T}}'_{*}$, where η_{n+1} is the radial return factor defined as $\frac{\tilde{\sigma}_{n+1}}{\tilde{\sigma}_{*}}$.

2.4. Kinematic, contact and thermal problems

The augmented Lagrangian formulation of Laursen and Simo is used to model contact and friction. This implementation of contact is discussed extensively in Srikanth and Zabaras (1999b). A radial return type algorithm (described above) is used for the time integration of the constitutive equations. The solution of a generic loading increment involves the solution to the principle of virtual work (PVW) given as follows:

$$\int_{\mathscr{B}_{\mathrm{r}}} \boldsymbol{P}_{\mathrm{r}}(\boldsymbol{F}_{\mathrm{r}}) \cdot \nabla_{\mathrm{r}} \tilde{\boldsymbol{u}} \, \mathrm{d}V_{\mathrm{r}} = \int_{\partial \mathscr{B}_{\mathrm{r}}} \boldsymbol{\lambda} \cdot \tilde{\boldsymbol{u}} \, \mathrm{d}A_{\mathrm{r}} + \int_{\mathscr{B}_{\mathrm{r}}} \boldsymbol{f} \cdot \tilde{\boldsymbol{u}} \, \mathrm{d}V_{\mathrm{r}} \tag{2.31}$$

for every admissible test function $\tilde{\boldsymbol{u}}$ expressed over the reference configuration $\mathscr{B}_{\mathrm{r}}$. The vector $\boldsymbol{\lambda}$ is the current contact traction expressed per unit area in $\Gamma \subset \partial \mathscr{B}_{\mathrm{r}}$. The weak form is solved in an incremental-iterative manner as a result of material as well as geometric non-linearities. The FEM is used for the solution of the weak form and bilinear quadrilateral elements are used along with the assumed strain analysis described in Srikanth and Zabaras (2001).

In the absence of external heat sources, the balance of energy in the current configuration, takes the form shown below (thermal sub-problem):

$$\rho c \frac{\partial \theta}{\partial t} = \mathscr{W}_{\text{mech}} - \nabla_{n+1} \cdot \boldsymbol{q} \tag{2.32}$$

The isotropic constitutive equation for the heat flux $\boldsymbol{q}$ is given by Fourier's law as follows:

$$\boldsymbol{q} = -K \nabla_{n+1} \theta \tag{2.33}$$

where the conductivity $K(\theta, L) \geqslant 0$. The mechanical dissipation $\mathscr{W}_{\text{mech}}$ is usually specified in terms of the plastic power by the following empirical law:

$$\mathscr{W}_{\text{mech}} = \omega \overline{\boldsymbol{T}} \cdot \overline{\boldsymbol{D}}^{\text{p}} = \omega \tilde{\sigma} \dot{\tilde{\epsilon}}^{\text{p}} \tag{2.34}$$

where $\omega \in [0.85, 0.95]$ is a constant dissipation factor that represents the fraction of the plastic work that is dissipated as heat. In this work, the non-dissipative latent heating is considered negligible in comparison to the mechanical dissipation $\mathscr{W}_{\text{mech}}$. An implicit Euler backward time-stepping scheme is used together with the classical Galerkin finite element formulation towards the solution of the thermal sub-problem.

3. Process optimization and its relation to the continuum sensitivity approach

Metal forming process design includes the control of complex, non-linear deformation mechanisms in order to achieve a desired objective that could consist of various criteria like, minimum work, desired shape or uniform deformation in the product and/or desired microstructure in the product. In this design procedure, we assume that the forming sequence is identified a priori and we focus on selecting the optimum design parameters in each of the operations/stages that make up the sequence. We introduce a gradient based optimization framework and the evaluation of the gradients of the objectives functions and constraints is performed through an innovative continuum sensitivity method (CSM) that is described next.

3.1. Definition of sensitivity in a continuum sensitivity framework

We briefly summarize the definitions of shape and parameter sensitivity of a Lagrangian field Ω, used in an updated Lagrangian (UL) framework. Sensitivity of any deformation or material state related field is the quantitative measure of the change in these fields as a result of infinitesimal perturbations to the process parameters (called parameter sensitivity), $\boldsymbol{\beta}_{\text{p}}$, or parameters that define the shape of the body (called shape sensitivity), $\boldsymbol{\beta}_s$. Let $\boldsymbol{\beta}_{\text{p}}$ ($\boldsymbol{\beta}$ in general for both shape as well as parameter sensitivities) denote the design variables related to process conditions which could be for example the die surface or the deformation rate. The dependence of the Lagrangian field $\Omega = \widehat{\Omega}(\boldsymbol{x}_n, t)$ on $\boldsymbol{\beta}_{\text{p}}$ can be expressed as follows:

$$\Omega = \widehat{\Omega}(\boldsymbol{x}_n, t; \boldsymbol{\beta}_{\text{p}}) = \widehat{\Omega}(\tilde{\boldsymbol{x}}(\boldsymbol{X}, t; \boldsymbol{\beta}_{\text{p}}), t; \boldsymbol{\beta}_{\text{p}}) = \widetilde{\Omega}(\boldsymbol{X}, t; \boldsymbol{\beta}_{\text{p}}) \tag{3.1}$$

The parameter sensitivity $\overset{\circ}{\Omega} = \overset{\circ}{\widehat{\Omega}}(\boldsymbol{x}_n, t; \boldsymbol{\beta}_{\text{p}}, \Delta\boldsymbol{\beta}_{\text{p}})$ is then defined as the total Gateaux differential of $\Omega = \widehat{\Omega}(\boldsymbol{x}_n, t; \boldsymbol{\beta}_{\text{p}})$ in the direction $\Delta\boldsymbol{\beta}_{\text{p}}$ computed at $\boldsymbol{\beta}_{\text{p}}$, i.e.,

$$\overset{\circ}{\widehat{\Omega}}(\boldsymbol{x}_n, t; \boldsymbol{\beta}_{\text{p}}, \Delta\boldsymbol{\beta}_{\text{p}}) = \overset{\circ}{\widetilde{\Omega}}(\boldsymbol{X}, t; \boldsymbol{\beta}_{\text{p}}, \Delta\boldsymbol{\beta}_{\text{p}}) = \frac{\mathrm{d}}{\mathrm{d}\lambda} \widetilde{\Omega}(\boldsymbol{X}, t; \boldsymbol{\beta}_{\text{p}} + \lambda \Delta\boldsymbol{\beta}_{\text{p}}) \Big|_{\lambda=0} \tag{3.2}$$

The shape sensitivity $\overset{\circ}{\Omega} = \overset{\circ}{\widehat{\Omega}}(\boldsymbol{x}_n, t; \boldsymbol{\beta}_s, \Delta\boldsymbol{\beta}_s)$ is defined (in a similar fashion to the parameter sensitivities) as the total directional differential of $\Omega = \widehat{\Omega}(\boldsymbol{x}_n, t; \boldsymbol{\beta}_s)$ in the direction $\Delta\boldsymbol{\beta}_s$ (perturbation to the design vector) computed at $\boldsymbol{\beta}_s$ (shape design vector)

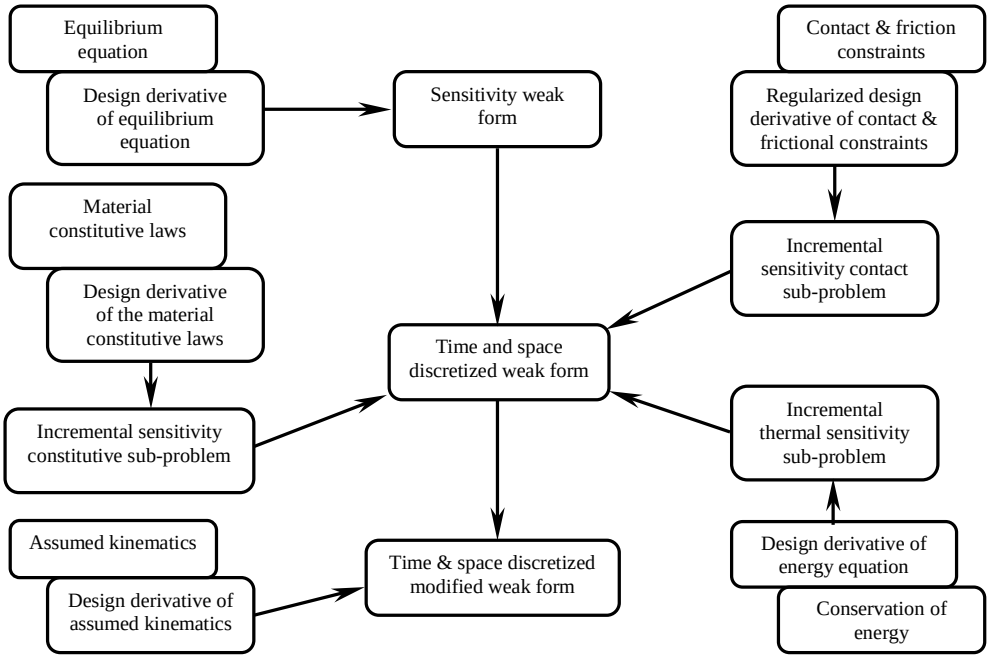

Fig. 1. Schematic of the continuum sensitivity algorithm in a generic forming stage.

$$\overset{\circ}{\widehat{\Omega}}(\boldsymbol{x}_n, t; \boldsymbol{\beta}_s, \Delta\boldsymbol{\beta}_s) = \overset{\circ}{\widetilde{\Omega}}(\boldsymbol{X}, t; \boldsymbol{\beta}_s, \Delta\boldsymbol{\beta}_s) = \overset{\circ}{\overline{\Omega}}(\boldsymbol{Y}, t; \boldsymbol{\beta}_s, \Delta\boldsymbol{\beta}_s) = \frac{\mathrm{d}}{\mathrm{d}\lambda}\overline{\Omega}(\boldsymbol{Y}, t; \boldsymbol{\beta}_s + \lambda\Delta\boldsymbol{\beta}_s)\Big|_{\lambda=0} \tag{3.3}$$

where $\boldsymbol{Y}$ is the material point in the design independent, reference material configuration $\mathscr{B}_R$ which results in the various initial configurations (preforms) $\mathscr{B}_0$ through a smooth, bijective, design-dependent mapping. This necessarily follows a domain parameterization approach in order to monitor the variation in the field due to the variation in the initial shape of the body. Specific information on shape and parameter sensitivities can be obtained from Ganapathysubramanian and Zabaras (2002, 2003), Badrinarayanan and Zabaras (1996), Zabaras et al. (2000), and Srikanth and Zabaras (2000). A definition of sensitivity fields in the context of a multi-stage forming process is given in Zabaras et al. (2003). The sensitivity framework adopted here is based on the design-differentiation of the direct continuum equations. This continuum sensitivity method (CSM) approach differs from other sensitivity methods available in the literature in that most methods are based on a design-differentiation of the discretized direct problem. Fig. 1 describes the various sub-problems involved in the CSM.

3.2. Sensitivity kinematic problem

In this section, the equations governing the sensitivity fields are computed at the continuum level. The sensitivity of the equilibrium equation is directly considered so as to establish a principle of virtual work like equation for the calculation of the sensitivity of deformation fields (Srikanth and Zabaras, 2000, 2001). Consistent with the above analysis, the sensitivity constitutive, sensitivity thermal and sensitivity contact equations are derived from the corresponding continuum equations rather than their numerically integrated counterparts. The sensitivity deformation problem is developed on the reference configuration $\mathscr{B}_\mathrm{r}$. The design differentiation of the equilibrium equation (2.10) results in the following:

$$\overset{\circ}{\overline{\nabla_{\mathrm{r}} \cdot \boldsymbol{P}_{\mathrm{r}}}} + \overset{\circ}{\boldsymbol{f}} = \boldsymbol{0} \quad \forall \boldsymbol{x}_{\mathrm{r}} \in \mathscr{B}_{\mathrm{r}} \ \forall t \in [t_n, t_{n+1}] \tag{3.4}$$

A variational form for the sensitivity equilibrium equation can be posed as follows (with the derivation following a similar procedure as that presented in Srikanth and Zabaras, 2000): calculate $\overset{\circ}{\boldsymbol{x}} = \overset{\circ}{\widehat{\boldsymbol{x}}}(\boldsymbol{x}_n, t; \boldsymbol{\beta}, \Delta\boldsymbol{\beta})$ such that

$$\int_{\mathscr{B}_{\mathrm{r}}} \overset{\circ}{\boldsymbol{P}}_{\mathrm{r}} \cdot \nabla_{\mathrm{r}} \tilde{\boldsymbol{\eta}} \, \mathrm{d}V_{\mathrm{r}} - \int_{\mathscr{B}_{\mathrm{r}}} \boldsymbol{P}_{\mathrm{r}} [\nabla_{\mathrm{r}} \cdot \boldsymbol{L}_{\mathrm{r}}^{\mathrm{T}}] \cdot \tilde{\boldsymbol{\eta}} \, \mathrm{d}V_{\mathrm{r}} - \int_{\mathscr{B}_{\mathrm{r}}} (\boldsymbol{P}_{\mathrm{r}} \boldsymbol{L}_{\mathrm{r}}^{\mathrm{T}} \cdot \nabla_{\mathrm{r}} \tilde{\boldsymbol{\eta}}) \, \mathrm{d}V_{\mathrm{r}} = \int_{\partial \mathscr{B}_{\mathrm{r}}} \left\{ \overset{\circ}{\boldsymbol{\lambda}} - [\boldsymbol{L}_{\mathrm{r}} \cdot (\boldsymbol{N} \otimes \boldsymbol{N})] \boldsymbol{\lambda} \right\} \cdot \tilde{\boldsymbol{\eta}} \, \mathrm{d}A_{\mathrm{r}} \tag{3.5}$$

for every $\tilde{\boldsymbol{\eta}}$, where $\tilde{\boldsymbol{\eta}}$ is a kinematically admissible sensitivity deformation field expressed over the reference configuration $\mathscr{B}_{\mathrm{r}}$. Also here, $\boldsymbol{\beta}$ is the design vector (can represent either $\boldsymbol{\beta}_{\mathrm{p}}$ or $\boldsymbol{\beta}_s$), $\Delta\boldsymbol{\beta}$ represents a perturbation to the design vector, $\boldsymbol{N}$ is the unit normal in $\partial\mathscr{B}_{\mathrm{r}}$ and $\boldsymbol{L}_{\mathrm{r}} \equiv \nabla_{\mathrm{r}} \overset{\circ}{\widehat{\boldsymbol{x}}}(\boldsymbol{x}_{\mathrm{r}}, t; \boldsymbol{\beta}, \Delta\boldsymbol{\beta}) = \overset{\circ}{\boldsymbol{F}}_{\mathrm{r}} \boldsymbol{F}_{\mathrm{r}}^{-1}$ refers to the design velocity gradient. In the case of parameter sensitivity analysis, the design velocity gradient at time t_0, $\boldsymbol{L}_0 = \boldsymbol{0}$. In the case of shape sensitivity analysis, the design velocity gradient at time t_0, $\boldsymbol{L}_0 = \nabla_0 \overset{\circ}{\widehat{\boldsymbol{X}}}(\boldsymbol{X}; \boldsymbol{\beta}_s, \Delta\boldsymbol{\beta}_s) = \overset{\circ}{\boldsymbol{F}}_R \boldsymbol{F}_R^{-1}$. The solution of this variational sensitivity problem involves evaluating the key relationships between $\overset{\circ}{\boldsymbol{P}}_{\mathrm{r}}$ and $[\overset{\circ}{\boldsymbol{F}}_{\mathrm{r}}, \overset{\circ}{\theta}]$ which is part of the constitutive sensitivity problem and between $\overset{\circ}{\boldsymbol{\lambda}}$ and $\overset{\circ}{\boldsymbol{x}}$, which is described by the sensitivity contact problem.

The relationship between $\overset{\circ}{\boldsymbol{P}}_{\mathrm{r}}$ and $[\overset{\circ}{\boldsymbol{x}}, \overset{\circ}{\theta}]$ is linear and is denoted as follows:

$$\overset{\circ}{\boldsymbol{P}}_{\mathrm{r}} = \mathscr{A}[\overset{\circ}{\boldsymbol{F}}_{\mathrm{r}}] + \mathscr{C} \overset{\circ}{\theta} + \mathscr{B} \tag{3.6}$$

where $\mathscr{A}$ is a fourth order tensor and $\mathscr{B}, \mathscr{C}$ are second order tensors, to be evaluated. These tensors will be shown to be constants, defined from known direct fields at the current time and sensitivity fields at the previous time step (see Section 3.3). The relationship between $\overset{\circ}{\boldsymbol{\lambda}}$ and $\overset{\circ}{\boldsymbol{x}}$ is non-trivial and obtained from the sensitivity contact problem as (Zabaras et al., 2000)

$$\overset{\circ}{\boldsymbol{\lambda}} = \boldsymbol{D}[\overset{\circ}{\boldsymbol{x}}] + \boldsymbol{d} \tag{3.7}$$

where $\boldsymbol{D}$ is a second order tensor and $\boldsymbol{d}$ a vector.

3.3. Sensitivity constitutive problem

In this constitutive sensitivity problem, the relationship between $\overset{\circ}{\boldsymbol{T}}$ and $\overset{\circ}{\boldsymbol{F}}_{n+1}$ and $\overset{\circ}{\theta}_{n+1}$ as required by the solution of the sensitivity thermo-mechanical problem is computed. As part of the update procedure, one further computes the set $[\overset{\circ}{\boldsymbol{T}}, \overset{\circ}{s}, \overset{\circ}{L}, \overset{\circ}{\boldsymbol{F}}^{\mathrm{e}}]$ at the end of the time increment t_{n+1} when the sensitivity of the total deformation gradient $\overset{\circ}{\boldsymbol{F}}_{n+1}$ and the sensitivity of the temperature field $\overset{\circ}{\theta}_{n+1}$ are given (evaluated). The sensitivity of the mechanical dissipation $\overset{\circ}{\mathscr{W}}_{\mathrm{mech}}$ is also computed as it is part of the driving force for the thermal sensitivity problem at time t_{n+1}.

The solution of the direct thermo-mechanical problem is known at time t_{n+1} i.e., the set $[\boldsymbol{T}, s, L, \boldsymbol{F}^{\mathrm{e}}]$, the body configuration $\mathscr{B}_{n+1}$ as well as the temperature field θ_{n+1} are known at t_{n+1}. Due to non-linear material response, the constitutive sensitivity problem is history dependent and the solution of the sensitivity problem at time t_n is assumed known, yielding the variables $[\overset{\circ}{\boldsymbol{T}}, \overset{\circ}{s}, \overset{\circ}{L}, \overset{\circ}{\boldsymbol{F}}^{\mathrm{e}}]$ at the beginning of the time increment $(t = t_n)$. It has been shown that the deformation sensitivity response does not explicitly depend on the history of the temperature sensitivity but is dependent only on the instantaneous temperature sensitivity response $\overset{\circ}{\theta}_{n+1}$ (Ganapathysubramanian and Zabaras, 2002). The solution of the sensitivity subproblem is advanced within the incremental solution scheme by integrating the evolution equations for the

sensitivity of the plastic and thermal deformation gradients, the evolution equation for the sensitivity of the state variable s and the grain size L. As part of this sub-problem, the linear relationship between $\overset{\circ}{\boldsymbol{T}}$ and $[\overset{\circ}{\boldsymbol{F}}, \overset{\circ}{\theta}]$ at time t_{n+1} is computed. This relationship will be used to compute in Eq. (3.6) the constants $\mathscr{A}$, $\mathscr{B}$ and $\mathscr{C}$ as needed in the solution of the sensitivity thermo-mechanical problem (Eq. (3.5)). The time integration scheme presented here is an Euler-backward time stepping algorithm.

3.3.1. Calculation of the linear relation between $\overset{\circ}{\boldsymbol{F}}{}^{p}_{n+1}$ and $[\overset{\circ}{\boldsymbol{F}}{}^{e}_{n+1}, \overset{\circ}{\theta}_{n+1}]$

The evolution equation for $\boldsymbol{F}^{\mathrm{p}}$ is given as, $\dot{\boldsymbol{F}}^{\mathrm{p}}(\boldsymbol{F}^{\mathrm{p}})^{-1} = \overline{\boldsymbol{D}}^{\mathrm{p}}$, assuming that the plastic spin $\overline{\boldsymbol{W}}^{\mathrm{p}} = 0$. Let us consider the design differentiation of this evolution equation. The sensitivity of the plastic stretching rate, $\overset{\circ}{\overline{\boldsymbol{D}}}{}^{\mathrm{p}}$, specifies completely $\overset{\circ}{\boldsymbol{F}}{}^{\mathrm{p}}$ (we herein drop the subscript $(n+1)$ for convenience):

$$\frac{\partial \overset{\circ}{\boldsymbol{F}}{}^{\mathrm{p}}}{\partial t} = \overline{\boldsymbol{D}}^{\mathrm{p}} \overset{\circ}{\boldsymbol{F}}{}^{\mathrm{p}} + \overset{\circ}{\overline{\boldsymbol{D}}}{}^{\mathrm{p}} \boldsymbol{F}^{\mathrm{p}} \tag{3.8}$$

$\overset{\circ}{\overline{\boldsymbol{D}}}{}^{\mathrm{p}}$ can be computed by taking the design-derivative of the flow rule (Eq. (2.9)):

$$\overset{\circ}{\overline{\boldsymbol{D}}}{}^{\mathrm{p}} = \frac{3}{2}\frac{f(\tilde{\sigma}, s, \theta)}{\tilde{\sigma}} \overset{\circ}{\overline{\boldsymbol{T}}}{}' + \frac{3}{2}\left(\frac{\tilde{\sigma} f_{\tilde{\sigma}} - f}{\tilde{\sigma}^2} \overset{\circ}{\tilde{\sigma}} + \frac{f_s}{\tilde{\sigma}} \overset{\circ}{s} + \frac{f_\theta}{\tilde{\sigma}} \overset{\circ}{\theta} + \frac{f_L}{\tilde{\sigma}} \overset{\circ}{L} \right) \overline{\boldsymbol{T}}' \tag{3.9}$$

where the subscripts denote partial derivatives and $\overset{\circ}{\overline{\boldsymbol{T}}}{}'$ is the deviatoric part of the sensitivity of the rotation neutralized Cauchy stress, $\overset{\circ}{\overline{\boldsymbol{T}}}$, and $\overset{\circ}{\tilde{\sigma}}$ is the sensitivity of the equivalent stress, i.e.,

$$\overset{\circ}{\overline{\boldsymbol{T}}} = \mathscr{L}^{\mathrm{e}}[\overset{\circ}{\overline{\boldsymbol{E}}}{}^{\mathrm{e}}] \tag{3.10}$$

$$\overset{\circ}{\tilde{\sigma}} = \frac{3}{2}\frac{\overset{\circ}{\overline{\boldsymbol{T}}}{}' \cdot \overline{\boldsymbol{T}}'}{\tilde{\sigma}} \tag{3.11}$$

One can further show that $\overset{\circ}{\overline{\boldsymbol{E}}}{}^{\mathrm{e}}$ is linearly related to $\overset{\circ}{\boldsymbol{F}}{}^{\mathrm{e}}$ as follows (Badrinarayanan and Zabaras, 1996):

$$\overset{\circ}{\overline{\boldsymbol{E}}}{}^{\mathrm{e}} = 4(\boldsymbol{U}^{\mathrm{e}} + \boldsymbol{I})^{-1} \overset{\circ}{\boldsymbol{U}}{}^{\mathrm{e}} (\boldsymbol{U}^{\mathrm{e}} + \boldsymbol{I})^{-1} \tag{3.12}$$

$$\overset{\circ}{\boldsymbol{U}}{}^{\mathrm{e}} = \mathrm{sym}\left\{ (\boldsymbol{U}^{\mathrm{e}})^{-1} \mathrm{sym}\left((\boldsymbol{F}^{\mathrm{e}})^{\mathrm{T}} \overset{\circ}{\boldsymbol{F}}{}^{\mathrm{e}} \right) \right\} \tag{3.13}$$

Thus from Eqs. (3.9)–(3.13), one can conclude that $\overset{\circ}{\overline{\boldsymbol{D}}}{}^{\mathrm{p}}$ depends explicitly only on $\overset{\circ}{\boldsymbol{F}}{}^{\mathrm{e}}$ and not on $\overset{\circ}{\boldsymbol{F}}{}^{\mathrm{p}}$.

The evolution equation for $\overset{\circ}{s}$ and $\overset{\circ}{L}$ is obtained by design differentiation of the evolution equation for the state variables (2.13) and (2.18):

$$\frac{\partial \overset{\circ}{s}}{\partial t} = g_{\tilde{\sigma}} \overset{\circ}{\tilde{\sigma}} + g_s \overset{\circ}{s} + g_\theta \overset{\circ}{\theta} + g_L \overset{\circ}{L} \tag{3.14}$$

$$\frac{\partial \overset{\circ}{L}}{\partial t} = l_{\tilde{\sigma}} \overset{\circ}{\tilde{\sigma}} + l_s \overset{\circ}{s} + l_\theta \overset{\circ}{\theta} + l_L \overset{\circ}{L} \tag{3.15}$$

The functions describing the evolution of the state variables, i.e., the deformation resistance and the grain size, are taken in this effort to be smooth enough to ensure differentiability. Any discontinuity/non-differentiability of these functions will need to be addressed through regularization.

The evolution equation for $\overset{\circ}{\boldsymbol{F}}{}^{\theta}$ is derived as follows (Ganapathysubramanian and Zabaras, 2002):

$$\overset{\circ}{\boldsymbol{F}}{}^{\theta} (\boldsymbol{F}^{\theta})^{-1} = \beta \overset{\circ}{\theta} \boldsymbol{I} \tag{3.16}$$

An Euler-backward integration scheme over (t_n, t_{n+1}) applied to the evolution equations for the sensitivities of the plastic deformation gradient (Eq. (3.8)), scalar state variables (Eqs. (3.14) and (3.15)) and thermal deformation gradient (Eq. (3.16)) yields:

- Sensitivity of the plastic deformation gradient at time t_{n+1}:

$$\overset{\circ}{\boldsymbol{F}}{}^{\mathrm{p}}(\boldsymbol{F}^{\mathrm{p}})^{-1} = \Delta\boldsymbol{F}^{\mathrm{p}}\overset{\circ}{\boldsymbol{F}}{}^{\mathrm{p}}_{n}(\boldsymbol{F}^{\mathrm{p}}_{n})^{-1}(\Delta\boldsymbol{F}^{\mathrm{p}})^{-1} + \Delta t\overset{\circ}{\overline{\boldsymbol{D}}}{}^{\mathrm{p}}_{n+1} \tag{3.17}$$

  where from the constitutive sub-problem of the direct problem,

$$\Delta\boldsymbol{F}^{\mathrm{p}} = \boldsymbol{F}^{\mathrm{p}}(\boldsymbol{F}^{\mathrm{p}}_{n})^{-1} = \exp(\Delta t\overline{\boldsymbol{D}}^{\mathrm{p}}) \tag{3.18}$$

  with $\Delta t = t_{n+1} - t_n$.
- Sensitivity of the scalar state variable s at time t_{n+1}:

$$\overset{\circ}{s} = \overset{\circ}{s}_n\frac{1}{1-\Delta t(g_s)} + \frac{(g_{\tilde{\sigma}})\Delta t}{1-\Delta t(g_s)}\overset{\circ}{\tilde{\sigma}} + \frac{(g_\theta)\Delta t}{1-\Delta t(g_s)}\overset{\circ}{\theta} + \frac{(g_L)\Delta t}{1-\Delta t(g_s)}\overset{\circ}{L} \tag{3.19}$$

- Sensitivity of the scalar state variable L at time t_{n+1}:

$$\overset{\circ}{L} = \overset{\circ}{L}_n\frac{1}{1-\Delta t(l_L)} + \frac{(l_{\tilde{\sigma}})\Delta t}{1-\Delta t(l_L)}\overset{\circ}{\tilde{\sigma}} + \frac{(l_s)\Delta t}{1-\Delta t(l_L)}\overset{\circ}{s} + \frac{(l_\theta)\Delta t}{1-\Delta t(l_L)}\overset{\circ}{\theta} \tag{3.20}$$

  From the above two equations, $\overset{\circ}{s}_{n+1}$ and $\overset{\circ}{L}_{n+1}$ can be evaluated as follows:

$$\overset{\circ}{s} = m_1 + m_2\overset{\circ}{\tilde{\sigma}} + m_3\overset{\circ}{\theta}, \qquad \overset{\circ}{L} = n_1 + n_2\overset{\circ}{\tilde{\sigma}} + n_3\overset{\circ}{\theta} \tag{3.21}$$

  where m_1, m_2, m_3, n_1, n_2, n_3 are constants that can be evaluated by solving the above mentioned system.
- Sensitivity of the thermal deformation gradient at time t_{n+1} (Ganapathysubramanian and Zabaras, 2002):

$$\overset{\circ}{\boldsymbol{F}}{}^{\theta} = \beta\overset{\circ}{\theta}\boldsymbol{F}^{\theta} \tag{3.22}$$

  Substituting Eqs. (3.9) and (3.21) in Eq. (3.17), one finally obtains that

$$\overset{\circ}{\boldsymbol{F}}{}^{\mathrm{p}}(\boldsymbol{F}^{\mathrm{p}})^{-1} = \boldsymbol{C}_{n+1} + a_{n+1}\overset{\circ}{\overline{\boldsymbol{T}}}{}' + b_{n+1}\overset{\circ}{\tilde{\sigma}}\overline{\boldsymbol{T}}' + c_{n+1}\overset{\circ}{\theta}\overline{\boldsymbol{T}}' \tag{3.23}$$

where

$$\begin{aligned}
&\boldsymbol{C}_{n+1} = \Delta\boldsymbol{F}^{\mathrm{p}}(\overset{\circ}{\boldsymbol{F}}{}^{\mathrm{p}}_{n}(\boldsymbol{F}^{\mathrm{p}}_{n})^{-1})(\Delta\boldsymbol{F}^{\mathrm{p}})^{-1} + \frac{3\Delta t}{2\tilde{\sigma}}(f_s m_1 + f_L n_1)\overline{\boldsymbol{T}}', \qquad a_{n+1} = \frac{3f\Delta t}{2\tilde{\sigma}},\\
&b_{n+1} = \frac{3}{2}\left\{\frac{\tilde{\sigma}(f_{\tilde{\sigma}}) - f}{\tilde{\sigma}^2} + \frac{(f_s)m_2}{\tilde{\sigma}} + \frac{(f_L)n_2}{\tilde{\sigma}}\right\}\Delta t, \qquad c_{n+1} = \frac{3}{2}\left(\frac{(f_s)m_3}{\tilde{\sigma}} + \frac{(f_L)n_3}{\tilde{\sigma}}\right)\Delta t
\end{aligned} \tag{3.24}$$

Eqs. (3.23) and (3.24) together with Eqs. (3.10)–(3.13) completely define the linear relation between $\overset{\circ}{\boldsymbol{F}}{}^{\mathrm{p}}_{n+1}$ and $[\overset{\circ}{\boldsymbol{F}}{}^{\mathrm{e}}_{n+1}, \overset{\circ}{\theta}_{n+1}]$.

3.3.2. Calculation of the linear relation between $\overset{\circ}{\boldsymbol{F}}{}^{e}_{n+1}$ and $[\overset{\circ}{\boldsymbol{F}}_{n+1}, \overset{\circ}{\theta}_{n+1}]$

Starting from the multiplicative decomposition of the deformation gradient, one can write (dropping the subscript $(n+1)$)

$$\overset{\circ}{\boldsymbol{F}} = \overset{\circ}{\boldsymbol{F}}{}^{\mathrm{e}}\boldsymbol{F}^{\mathrm{p}}\boldsymbol{F}^{\theta} + \boldsymbol{F}^{\mathrm{e}}\overset{\circ}{\boldsymbol{F}}{}^{\mathrm{p}}\boldsymbol{F}^{\theta} + \boldsymbol{F}^{\mathrm{e}}\boldsymbol{F}^{\mathrm{p}}\overset{\circ}{\boldsymbol{F}}{}^{\theta} \tag{3.25}$$

Hence,

$$(\boldsymbol{F}^{\mathrm{e}})^{-1}(\overset{\circ}{\boldsymbol{F}}\boldsymbol{F}^{-1})\boldsymbol{F}^{\mathrm{e}} = (\boldsymbol{F}^{\mathrm{e}})^{-1}\overset{\circ}{\boldsymbol{F}}^{\mathrm{e}} + \overset{\circ}{\boldsymbol{F}}^{\mathrm{p}}(\boldsymbol{F}^{\mathrm{p}})^{-1} + \beta\overset{\circ}{\theta}\boldsymbol{I} \tag{3.26}$$

Using Eqs. (3.13) and (3.10), it has been shown that $\overset{\circ}{\overline{\boldsymbol{T}}}'_{n+1}$ and $\overset{\circ}{\tilde{\sigma}}_{n+1}$ linearly depend on $\overset{\circ}{\boldsymbol{F}}^{\mathrm{e}}_{n+1}$. Therefore substitution of Eq. (3.23) in Eq. (3.26) results in a linear relation between $\overset{\circ}{\boldsymbol{F}}^{\mathrm{e}}$ and $[\overset{\circ}{\boldsymbol{F}}, \overset{\circ}{\theta}]$:

$$(\boldsymbol{F}^{\mathrm{e}})^{-1}(\overset{\circ}{\boldsymbol{F}}\boldsymbol{F}^{-1})\boldsymbol{F}^{\mathrm{e}} - \boldsymbol{C}_{n+1} = (\boldsymbol{F}^{\mathrm{e}})^{-1}\overset{\circ}{\boldsymbol{F}}^{\mathrm{e}} + a_{n+1}\overset{\circ}{\overline{\boldsymbol{T}}}' + b_{n+1}\overset{\circ}{\tilde{\sigma}}\overline{\boldsymbol{T}}' + [c_{n+1}\overline{\boldsymbol{T}}' + \beta\boldsymbol{I}]\overset{\circ}{\theta} \tag{3.27}$$

The linear relationship above can be expressed as (incorporating the subscript $(n+1)$)

$$\overset{\circ}{\boldsymbol{F}}^{\mathrm{e}}_{n+1} = \mathscr{A}(\boldsymbol{V}_{n+1})[\overset{\circ}{\boldsymbol{F}}_{n+1}] + \boldsymbol{A}(\boldsymbol{V}_{n+1}, \overset{\circ}{\boldsymbol{V}}_n) + \boldsymbol{B}(\boldsymbol{V}_{n+1})\overset{\circ}{\theta}_{n+1} \tag{3.28}$$

where $\boldsymbol{A}$ and $\boldsymbol{B}$ are second order tensor functions, $\mathscr{A}$, a fourth order tensor function and $\boldsymbol{V} \equiv [\boldsymbol{T}, s, L, \boldsymbol{F}^{\mathrm{p}}]$.

3.3.3. Calculation of the linear relation between $\overset{\circ}{\mathscr{W}}_{mech}$ and $[\overset{\circ}{\boldsymbol{F}}_{n+1}, \overset{\circ}{\theta}_{n+1}]$

Using Eq. (2.34), we can compute $\overset{\circ}{\mathscr{W}}_{\mathrm{mech}}$ as follows (once again, we drop the subscript $(n+1)$):

$$\overset{\circ}{\mathscr{W}}_{\mathrm{mech}} = \omega(\overset{\circ}{\tilde{\sigma}}f + \tilde{\sigma}\overset{\circ}{f}) = \omega[(f + \tilde{\sigma}f_{\tilde{\sigma}})\overset{\circ}{\tilde{\sigma}} + \tilde{\sigma}f_s\overset{\circ}{s} + \tilde{\sigma}f_\theta\overset{\circ}{\theta} + \tilde{\sigma}f_L\overset{\circ}{L}] \tag{3.29}$$

Using the elastic moduli from Eqs. (2.7), (3.10) and (3.11), one can prove the following:

$$\overset{\circ}{\tilde{\sigma}} = \frac{3\mu}{\tilde{\sigma}}\overset{\circ}{\overline{\boldsymbol{E}}}^{\mathrm{e}'} \cdot \overline{\boldsymbol{T}}' = \frac{3\mu}{\tilde{\sigma}}\overset{\circ}{\boldsymbol{E}}^{\mathrm{e}} \cdot \overline{\boldsymbol{T}}' \tag{3.30}$$

and

$$\overset{\circ}{\tilde{\sigma}} = \frac{3\mu(\boldsymbol{G} \cdot \overline{\boldsymbol{T}}') - 2\mu c_{n+1}\tilde{\sigma}^2\overset{\circ}{\theta}}{\tilde{\sigma}(1 + 2\mu(a_{n+1} + \tilde{\sigma}b_{n+1}))} \tag{3.31}$$

where $\boldsymbol{G}$ is the LHS of Eq. (3.27).

One finally obtains the following expression for $\overset{\circ}{\mathscr{W}}_{\mathrm{mech}}$ at t_{n+1}:

$$\overset{\circ}{\mathscr{W}}_{\mathrm{mech},n+1} = \boldsymbol{K}(\boldsymbol{V}_{n+1}) \cdot \overset{\circ}{\boldsymbol{F}}_{n+1} + \boldsymbol{k}_1(\boldsymbol{V}_{n+1}, \overset{\circ}{\boldsymbol{V}}_n) + \boldsymbol{k}_2(\boldsymbol{V}_{n+1})\overset{\circ}{\theta}_{n+1} \tag{3.32}$$

where $\boldsymbol{K}$ is a second order tensor function and $\boldsymbol{k}_1, \boldsymbol{k}_2$ are scalars. The sensitivity thermal problem and the contact sensitivity problems are dealt the same way as described in Ganapathysubramanian and Zabaras (2002).

The next section deals with numerical analysis and involves the comparison of the direct solution with results available experimentally. A validation of the sensitivity analysis is also provided and several design optimization problems are addressed. More details on how the present methodology can be incorporated in a multi-stage process design can be obtained from Zabaras et al. (2003).

4. Numerical accuracy studies and design examples

Some numerical examples are considered to validate and study the performance of the proposed direct, sensitivity and design algorithms. The computations were performed using Intel processors on the Cornell Theory Center's AC^3 Velocity configuration. In all reported axially symmetric simulations, the a priori stabilized $\boldsymbol{F}$-bar method with a stabilization parameter $\epsilon = 10^{-03}$ was implemented for 4-noded quadrilateral elements (Srikanth and Zabaras, 2001). The die is assumed to be fixed and the workpiece moves towards the die with a prescribed velocity in all the following examples. The workpiece material is taken to

be 0.2% C Steel (cast) at an initial temperature of 1213 K, with a mean grain size of 91 μm. The specific constitutive model used is defined by Eqs. (2.12), (2.13) and (2.18). The specific values of the mechanical and thermal parameters are given in Table 1. In the various optimization problems defined in the examples, a penalty method was used to convert a constrained optimization problem to an unconstrained one. Furthermore, a quasi-Newton type algorithm was used to solve the unconstrained problem and the BFGS scheme (Nocedal and Wright, 1999) to update the Hessian of the objective function. In the examples to be considered, the following thermal boundary conditions were imposed. Convective boundary conditions are imposed on all free surfaces, i.e., surfaces other than symmetry axes, that are not in contact. The convective heat transfer coefficient is taken as $h = 6.7$ W/(m^2 K). The ambient (atmospheric) temperature is taken as 298 K. For simplicity, the die is assumed to be rigid and no heat transfer is considered between the die and the workpiece.

In the following examples, upset forging between parallel dies of a right cylindrical billet (axisymmetric analysis) is considered. A sample optimization problem is described in Fig. 2 (Ganapathysubramanian and Zabaras, 2003). Further, the various die and preform shapes were approximated with Bézier curves and the design variables were selected to be the corresponding scalars in these approximations. The free surface of the preform shown in Fig. 2 and labelled, $R_{\boldsymbol{\beta}}(\alpha)$, is represented with a degree six Bézier curve (with seven Bernstein basis functions). Using the restriction on the slope due to symmetry, i.e., $R'_{\boldsymbol{\beta}}(0) = 0$, the representation of $R_{\boldsymbol{\beta}}$ can be defined with six independent design variables β_i, $i = 1, \ldots, 6$ as follows:

$$R_{\boldsymbol{\beta}}(\alpha) = \sum_{i=1}^{6} \beta_i \phi_i(\alpha), \quad Z = 1.5\alpha, \qquad 0 \leqslant \alpha \leqslant 1 \tag{4.1}$$

where Z represents the axial coordinate and the Bernstein basis functions are given as

Table 1
Material parameters for 0.2% C steel at 1213 K (Busso, 1998)

Material parameter	Value
$\dot{\bar{\epsilon}}_0$	2.618×10^{11} s^{-1}
$\mathscr{Q}$	283 kJ mol^{-1}
μ	57.69 GPa
κ	125.0 GPa
K	32.5 N/(s K)
ρc	4.884 MN/(m^2 K)
ω	0.90
L_0	91.0 μm
w	2.9
ζ	0.308
n_1	0.11
s_0	150.0 MPa
χ	431 MPa
h_s	7800
a_s	1.55
n_2	0.069
f_R	120
f_C	0.728
C_R	59
C_c	59
p	0.8
q	5 N mm^{p-2}
f_X	1.0
$\dot{L}_0$	6.0×10^6 m s^{-1}

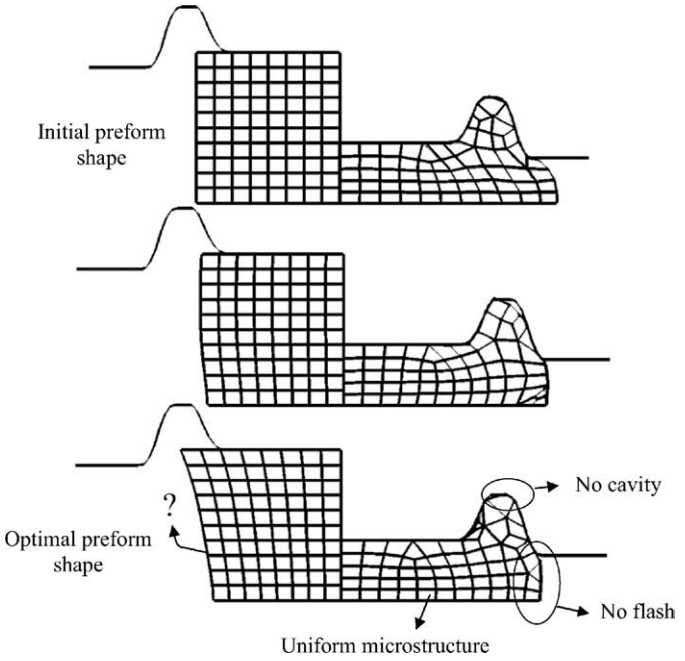

Fig. 2. A schematic describing a hypothetical preform design problem along with some possible optimization objectives.

$$\phi_1 = (1.0-\alpha)^5(1.0+5.0\alpha), \qquad \phi_2 = 15.0(1.0-\alpha)^4\alpha^2, \qquad \phi_3 = 20.0(1.0-\alpha)^3\alpha^3,$$
$$\phi_4 = 15.0(1.0-\alpha)^2\alpha^4, \qquad \phi_5 = 6.0(1.0-\alpha)\alpha^5, \qquad \phi_6 = \alpha^6 \tag{4.2}$$

4.1. Specific material characterization

The specific constitutive model chosen is presented in Busso (1998). The material chosen for the analysis following this section (0.2% C steel) has the evolution of the equivalent plastic strain (Eq. (2.12)) defined as follows:

$$\dot{\bar{\epsilon}}^{\mathrm{p}} = \dot{\tilde{\epsilon}}_0 \exp\left(\frac{-\mathcal{Q}}{R\theta}\right)\left(\frac{L_0}{L}\right)^{w}\left[\sinh\left(\frac{\tilde{\sigma}}{\zeta s}\right)\right]^{1/n_1} \tag{4.3}$$

where the material parameters are defined in Table 1. The evolution of the deformation resistance, i.e., the hardening law is defined by the following equation:

$$h(\tilde{\sigma}, s, \theta, L) = h_s\left|1-\frac{s}{s^*}\right|^{a_s}\operatorname{sign}\left(1-\frac{s}{s^*}\right)\dot{\bar{\epsilon}}^{\mathrm{p}} \tag{4.4}$$

where s^*, the dynamically stable value of s, is defined as

$$s^* = \chi\left\{\frac{\dot{\bar{\epsilon}}^{\mathrm{p}}}{\dot{\tilde{\epsilon}}_0}\exp\left(\frac{\mathcal{Q}}{R\theta}\right)\left(\frac{L^*}{L_0}\right)^{w}\right\}^{n_2} \tag{4.5}$$

where χ and n_2 are material parameters.

The kinetics of grain growth are defined through the evolution of the mean grain size as

$$\dot{L} = -f_R X_R \prec L - L^* \succ \dot{\bar{\epsilon}}^{\mathrm{p}} + \dot{L}_0 (1 - \exp(- \prec X_R - X_{Rc} \succ)) \exp\left(-\frac{\mathcal{Q}}{R\theta}\right)\left(\frac{L_0}{L}\right) \tag{4.6}$$

where f_R, $\dot{L}_0$ are material constants and X_R denotes the volume fraction of grains recrystallized. The volume fraction of grains recrystallized is given through the following expression:

$$X_R = 1 - \exp\{-A_L \dot{L}_{\mathrm{rec}} t_R\} \tag{4.7}$$

where t_R is the recrystallization time, A_L is the mean grain and sub-grain boundary area per unit volume which is active and capable of nucleation, and $\dot{L}_{\mathrm{rec}}$ the mean rate of grain refinement during recrystallization. The above expression is simplified to obtain (Busso, 1998):

$$X_R = 1 - \exp\left\{ - f_X \frac{L_0}{L^*} \left\langle \frac{\tilde{\epsilon}^{\mathrm{p}} - \tilde{\epsilon}^{\mathrm{p}}_C}{\dot{\bar{\epsilon}}^{\mathrm{p}}} \right\rangle \right\} \tag{4.8}$$

Furthermore, the critical strain for the onset of recrystallization is given by

$$\tilde{\epsilon}^{\mathrm{p}}_C = \frac{2}{\sqrt{3}} \frac{C_{\mathrm{c}}}{\mu} (f_C S^* - S_0) \tag{4.9}$$

where C_{c}, f_C are prescribed material parameters. In addition, $\tilde{\epsilon}^{\mathrm{p}}_R$ is given by

$$\tilde{\epsilon}^{\mathrm{p}}_R = \frac{2}{\sqrt{3}} \frac{C_R}{\mu} S_0^* \prec \left(\frac{L^w - L^{*^w}}{L_0^w} \right) \succ \tag{4.10}$$

Additionally, an implicit relation (Busso, 1998) for the dynamically stable recrystallized mean grain size in terms of the strain rate, the absolute temperature and the initial grain size is given as follows:

$$L^* = \left(\frac{q}{\zeta \chi A^{n_2}} \right)^{1/p} \left\{ \ln(A^{n_1} + \sqrt{A^{2n_1} + 1}) \right\}^{-1/p} \tag{4.11}$$

where

$$A = \frac{\dot{\bar{\epsilon}}^{\mathrm{p}}}{\dot{\epsilon}_0} \frac{L^{*w}}{L_0} \exp\left(\frac{\mathcal{Q}}{R\theta}\right) \tag{4.12}$$

A Newton type iterative procedure is used to evaluate L^* given the values of $\dot{\bar{\epsilon}}^{\mathrm{p}}$, θ and L_0.

4.2. Verification of direct analysis (Example 1)

A simulation is performed to obtain the uni-axial stress–strain response of the material at different strain rates. These strain rates were chosen to be exactly those used in Busso (1998), so that an accuracy check can be performed with the reported experimental results. These rates are 2.8×10^{-4}, 4.5×10^{-3}, 1.8×10^{-2} and 0.15 s^{-1}. The measured grain size as well as the predicted grain sizes for 0.2% C steel are summarized in Table 2. In addition to the evolution of the mean grain size, the stress–strain response is also shown in Fig. 3. The proposed theory clearly describes a rapid decrease in mean grain size following the onset of primary recrystallization for the higher strain rates. In addition, a good agreement of the steady state values of the grain size is observed for these strain rates. It is, though, observed that the model prediction for low strain rates is not accurate. One plausible reason for such behavior is that the mean grain size does not attain a quasi-steady state value towards the end of primary recrystallization (involves multiple peak recrystallization according to Busso, 1998). In other words, recrystallization is much lower than grain growth when it should have been the other way around.

Table 2
Measured and predicted mean grain sizes (in μm) for 0.2% C steel (cast)

Strain rate (s^{-1})	0.2% C steel	
	Measured	Predicted
0.15	45.8	40.2
1.8×10^{-2}	51.9	47.7
4.5×10^{-3}	55.9	57.1
2.8×10^{-4}	56.2	102.1

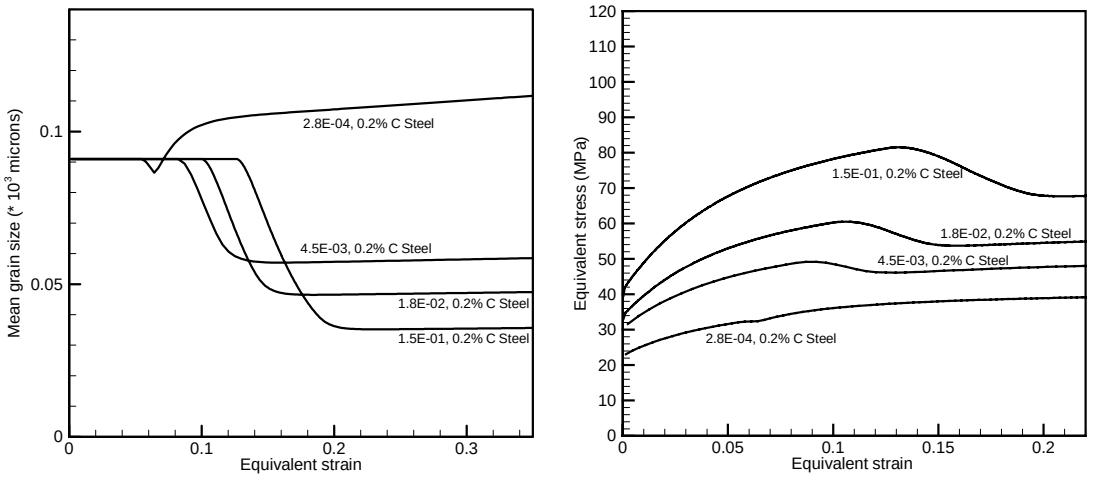

Fig. 3. The predicted evolution of the mean grain size and the material response in uni-axial tension at various strain rates (Example 1).

4.3. Validation of the thermomechanical sensitivity analysis (Example 2)

This section involves the validation of the shape sensitivity analysis for a thermo-mechanical process by a comparison with the forward finite difference method (FDM). Upset forging is considered between parallel flat dies of a cylindrical billet (axisymmetric) 2 mm in diameter and 3 mm in height. The initial billet was subject to a large height reduction of 33.34% in 500 s using a fixed time step of $\Delta t = 1.0$ s at a nominal strain rate of 0.001 s^{-1}. The preform free surface is represented as in Eq. (4.1). The shape parameters in the reference preform (cylindrical billet) are $\beta_i = 1.0$ mm, $i = 1, \ldots, 6$. Shape sensitivities are taken with respect to the free surface shape which is altered by perturbing the design variable β_3. Analysis is performed using the UL formulation with the coefficient of friction taken as 0.4. Fig. 4 depicts the distribution of the equivalent stress, equivalent scalar state variable, temperature, mean grain size and the fraction recrystallized in the deformed workpiece at the final time, $t = 500$ s. This solution defines the reference solution at which the sensitivity fields will be computed for a specified perturbation in the design variables.

Figs. 5–7 show at $t = 500$ s the shape sensitivity of the state variable, temperature and the mean grain size, respectively, using the CSM and FDM sensitivity computations.

The FDM sensitivity results are obtained using the results of the direct analysis and a forward difference approximation for a perturbation of the design variable, β_3, by $\Delta\beta_3 = 10^{-04}$ mm. Thus these results validate the proposed continuum sensitivity analysis.

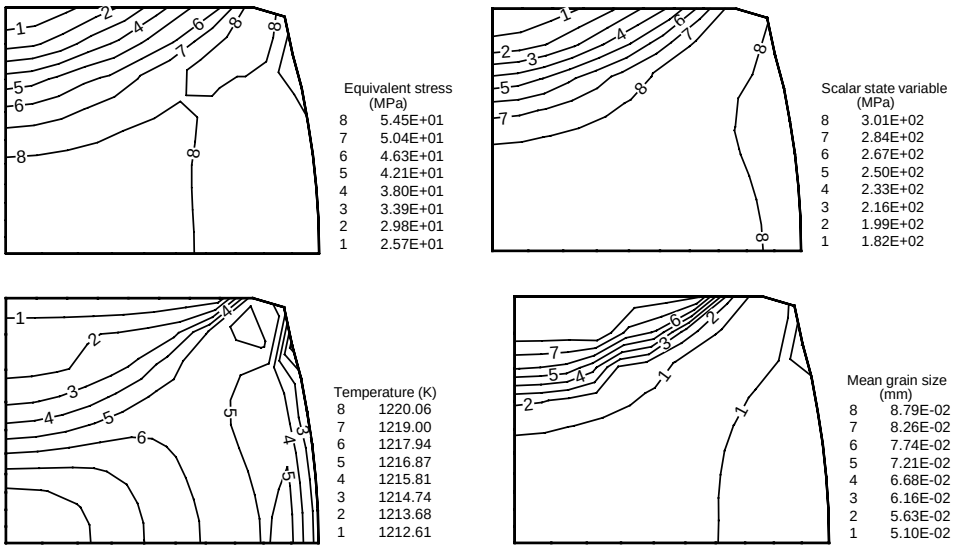

Fig. 4. Solution of the reference problem: the spatial variation of the equivalent stress, scalar state variable, temperature and grain size at $t = 500$ s (Example 2).

4.4. Design optimization examples using the CSM

4.4.1. Preform design in open-die forging to minimize barrelling and the deviation of the mean grain size (Example 3)

The objective here is to design the shape of a cylindrical preform of height 3.0 mm and fixed volume, that when compressed with a flat die in an open-die forging process yields a circular cylinder of radius $r_0 = 1.224$ mm and height 2.0 mm, i.e., a final product of a given height with no barrelling. In addition, we are interested to minimize the deviation in the mean grain size in the entire workpiece. The initial design (preform shape) is chosen to correspond to that of a right circular cylinder with uniform radius 1.0 mm (computed assuming volume conservation during deformation). The free surface $R_{\boldsymbol{\beta}}(\alpha)$ is represented with a degree 6 Bézier curve as given in Eq. (4.1). The finite dimensional optimization problem is posed as follows:

$$\min_{\boldsymbol{\beta}} \mathscr{F}(\boldsymbol{\beta}) = \frac{\lambda_1}{N_1} \sum_{i=1}^{N_1} (x_1^i(\boldsymbol{\beta}) - r_0)^2 + \frac{\lambda_2}{N_2} \sum_{i=1}^{N_2} (L^i(\boldsymbol{\beta}) - \prec L(\boldsymbol{\beta}) \succ)^2 \tag{4.13}$$

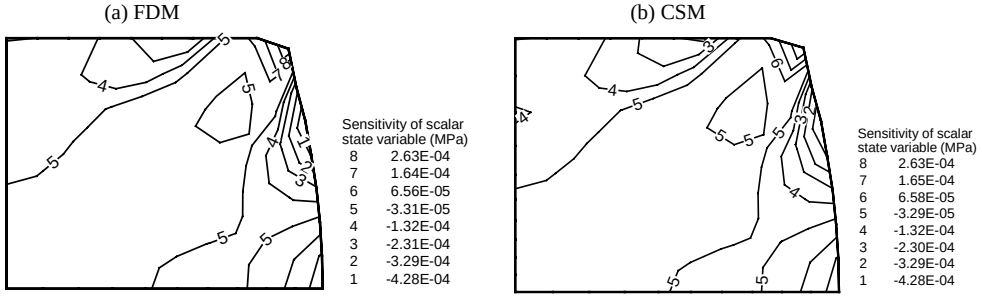

Fig. 5. Shape sensitivity of the scalar state variable at $t = 500$ s computed using the FDM and CSM methods (Example 2).

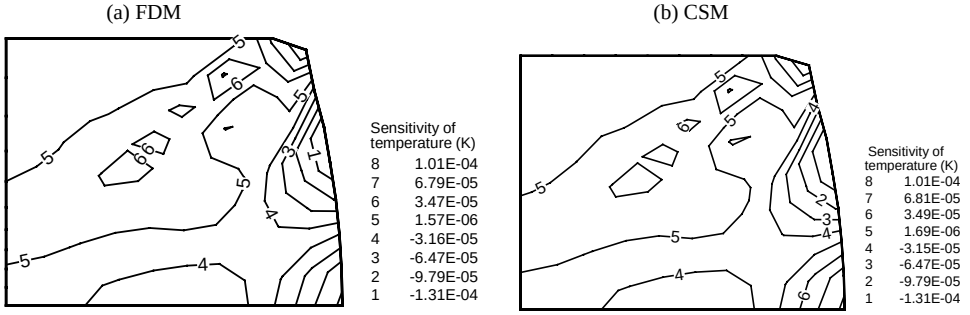

Fig. 6. Spatial variation of the shape sensitivity of the temperature at $t = 500$ s computed using the FDM and CSM methods (Example 2).

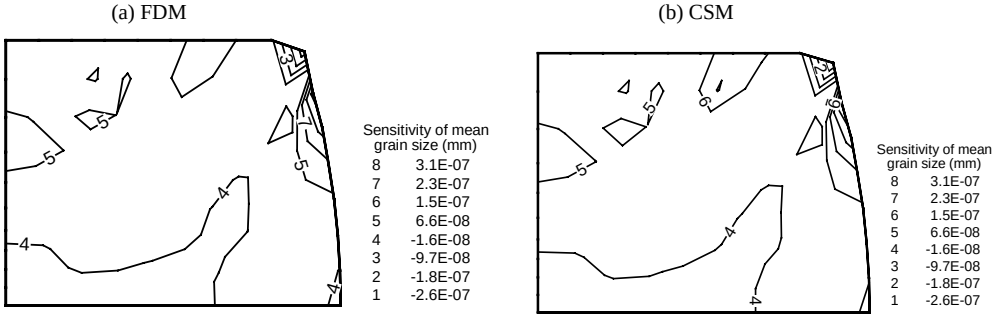

Fig. 7. Spatial variation of the shape sensitivity of the mean grain size at $t = 500$ s computed using the FDM and CSM methods (Example 2).

where $\boldsymbol{\beta} = \{\beta_1, \ldots, \beta_6\}$ and N_1, N_2 refer to the number of nodes on the free surface of the final product (which can vary between optimization iterations). The total number of measuring points for the grain size is here taken as the total number of Gauss integration points. λ_1, λ_2 are taken as $1.0\mathrm{E}+04$ and $1.0\mathrm{E}+06$ mm^{-2}, respectively, by considering the ratio of the two objectives at the end of the initial deformation problem. The initial and all subsequently obtained preforms were discretized with a 6×8 mesh for the quarter geometry shown in Fig. 8. The variation of the objective function with the iteration index is shown in Fig. 9. The optimal preforms and the product obtained is shown in Fig. 10. Also shown in Fig. 11 is the variation of the variance of the mean grain size with optimization iterations.

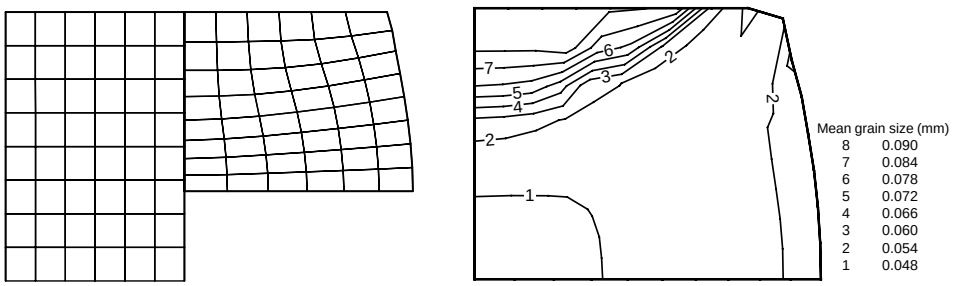

Fig. 8. Guess preform and grain size distribution in product for the thermo-mechanical preform forging design problem (Example 3).

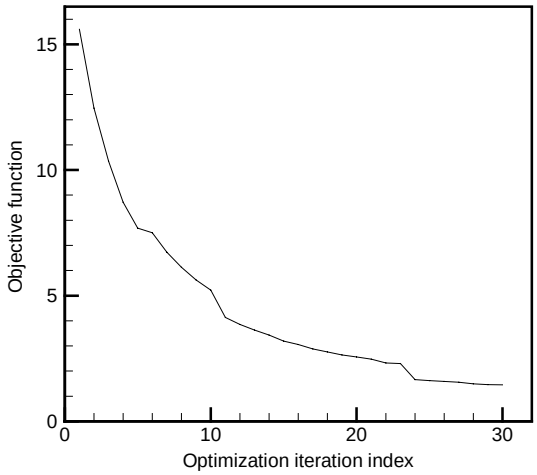

Fig. 9. Variation of the objective function versus the optimization iteration (Example 3).

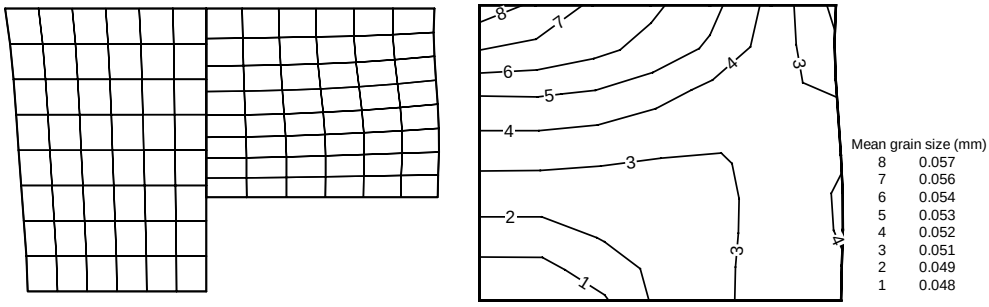

Fig. 10. Optimal preform and grain size distribution in final product for the thermo-mechanical preform design problem (Example 3).

4.4.2. Die design for extrusion (Example 4)

This problem involves the design of the extrusion die shape so as to minimize the deviation of the grain size at the exit. Here, we design an extrusion process with a die of area reduction of 12.0%. The initial radius of the workpiece is 0.5 mm. It was extruded with a nominal displacement rate of 0.001 s^{-1}. A total of 600 time steps were performed to reach steady-state conditions at the exit. A coefficient of friction of 0.01 was assumed at the die–workpiece interface. The symmetry of the problem allowed modelling only half of the geometry. The die surface is represented by a degree six ($n = 6$) Bézier curve as follows:

$$r(\alpha) = \sum_{i=1}^{n+1} C_i \phi_i(\alpha), \quad z = 0.3\alpha \text{ in mm} \quad 0 \leqslant \alpha \leqslant 1 \tag{4.14}$$

where C_i, $i = 1, \ldots, (n+1)$, are the algebraic control parameters. The Bernstein functions $\phi_i(\alpha)$ are given as

$$\phi_1 = (1.0-\alpha)^6, \qquad \phi_2 = 6.0(1.0-\alpha)^5\alpha, \qquad \phi_3 = 15.0(1.0-\alpha)^4\alpha^2,$$
$$\phi_4 = 20.0(1.0-\alpha)^3\alpha^3, \qquad \phi_5 = 15.0(1.0-\alpha)^2\alpha^4, \qquad \phi_6 = 6.0(1.0-\alpha)\alpha^5, \qquad \phi_7 = \alpha^6 \tag{4.15}$$

In order to obtain the same reduction for different die design parameters, the radius and slope (with respect to the z-axis) at the inlet and exit are fixed (slope is taken as 0):

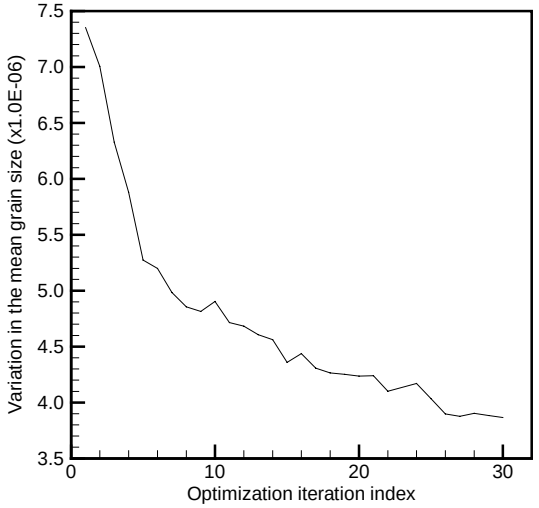

Fig. 11. Plot representing the average variation (in the mean grain sizes through out the final product) with the optimization iteration index (Example 3).

$$C_1 = 0.5 \text{ mm} \tag{4.16}$$

$$C_7 = 0.46 \text{ mm} \tag{4.17}$$

$$C_2 = C_1 \tag{4.18}$$

$$C_6 = C_7 \tag{4.19}$$

With this selection of parameters, there are three die design parameters left. The initial (reference) values are arbitrary and are selected as $C_3 = 0.475$, $C_4 = 0.475$, and $C_5 = 0.475$ (all of them in mm).

The finite dimensional optimization problem is posed as follows:

$$\min_{\boldsymbol{\beta}} \mathscr{F}(\boldsymbol{\beta}) = \frac{1}{N} \sum_{i=1}^{N} (l^i(\boldsymbol{\beta}) - \prec l(\boldsymbol{\beta}) \succ)^2 \tag{4.20}$$

where $\boldsymbol{\beta} = \{\beta_1, \ldots, \beta_3\}$, l^i is the non-dimesionalized mean grain size (non-dimesionalized using the initial grain size of 91 μm). The area of interest is defined as the volume at the exit (specified radius 0.45 mm), every point of which has a z-axis coordinate of greater than 0.3 mm. N refers to the total number of sampling nodal points in the region of interest. A perturbation of 10^{-3} mm is used for evaluating the sensitivities with respect to the die shape.

Fig. 12 shows the variation of the die shape with iterations. The variation of the objective function with the iteration index is shown in Fig. 13. In Fig. 14, we compare the grain sizes of the extruded product at various iterations—i.e., with different die shapes. The maximum grain size and the average grain size in the product obtained using the guess die shape was observed to be approximately 234 and 130 μm, respectively. Thus the guess die shape leads to a huge increase in grain size in the extruded product (from an initial grain size of 91 μm). This leads to a large variation in the mean grain size in the extruded product. In the product obtained using the optimum die shape, an average grain size of 144 μm and a variation of about 80 μm was observed. The variance is nearly halved as seen in Fig. 13 that presents the objective function.

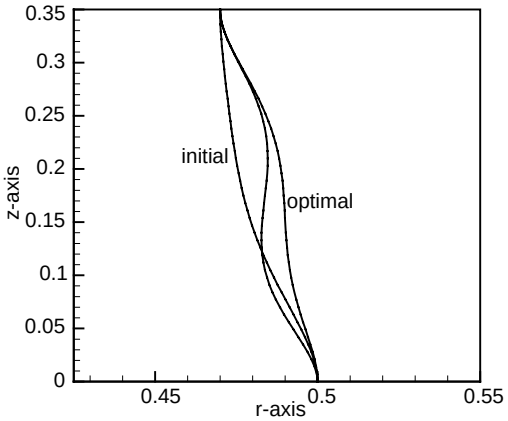

Fig. 12. The variation of the die shape about some iterations (Example 4).

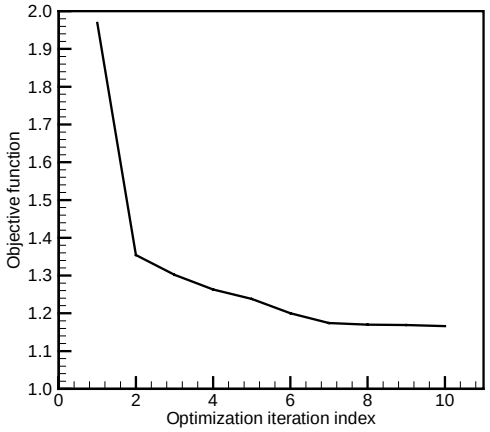

Fig. 13. The variation of the objective with iteration index (Example 4).

4.4.3. Two-stage forging process design (Example 5)

This example presents a forging process design for producing an axisymmetric disk in two stages. The initial billet is a right cylinder of 1.6 mm height and 1.04 mm radius. The height reduction at $r = 0$, in the first stage is 0.3 mm and in the second stage is 0.4 mm. A quarter of the billet is modelled in the simulation and design. The friction coefficient in the preforming and finishing stages is taken as 0.2. The material is assumed to be 0.2% C Steel at an initial temperature of 1213 K. The material properties are the same as those used in the previous examples. The design problem involves a preforming stage using a flat die in an open-die forging process. The finishing stage is a closed die of desired shape. The volume of the billet is chosen so that the final product occupies the finishing die completely.

The preforming die surface is represented using a degree six Bézier curve with five independent variables.

$$r(\alpha) = 0.9\alpha, \qquad z_\beta(\alpha) = \sum_{i=1}^{7} \beta_i \phi_i(\alpha) \tag{4.21}$$

The die height at $r = 0$ was specified and the die shape is assumed to have a zero slope at $r = 0$. The following basis functions are assumed:

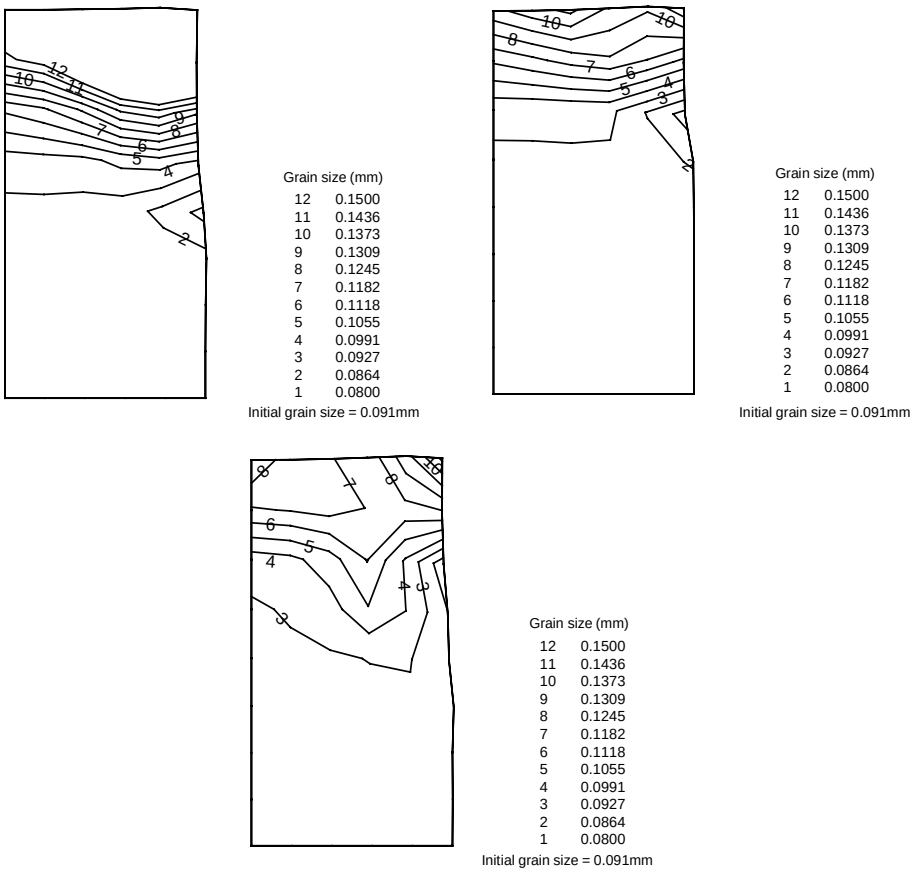

Fig. 14. Variation in grain sizes in the extruded product obtained at different iterations during the design process (Example 4).

$$\phi_1 = (1-\alpha)^6, \qquad \phi_2 = 6(1-\alpha)^5\alpha, \qquad \phi_3 = 15(1-\alpha)^4\alpha^2, \qquad \phi_4 = 20(1-\alpha)^3\alpha^3,$$
$$\phi_5 = 15(1-\alpha)^2\alpha^4, \qquad \phi_6 = 6(1-\alpha)\alpha^5, \qquad \phi_7 = \alpha^7 \tag{4.22}$$

We herein choose β_6 and $\beta_7 = 0.9$ mm, in order to fix the height and slope at $r = 0$.

In addition, the finishing die is defined as follows:

$$\text{shape}(\eta) = \begin{cases} r(\eta) = 1.3 \ * \ (1-\eta) \\ z(\eta) = \begin{cases} 70.6 \ * \ \eta^3 + 1.35 & \eta \in [0, 0.08] \\ -416.2 \ * \ (\eta - 0.17)^3 + 1.9 & \eta \in [0.08, 0.17] \\ 1.90 & \eta \in [0.17, 0.37] \\ 15.9 - 79.4 \ * \ \eta + 295.9 \ * \ \eta^2 & \\ -511.9 \ * \ \eta^3 + 403.4 \ * \ \eta^4 & \\ -118.1 \ * \ \eta^5 & \eta \in [0.37, 1] \end{cases} \end{cases}$$

We are here interested to design the preforming die shape so that the variation in the grain sizes in the finished product is minimized. Mathematically, this is represented as follows:

$$\min_{\boldsymbol{\beta}} \mathscr{F}(\boldsymbol{\beta}) = \frac{1}{\omega * N} \sum_{i=1}^{N} (L_i(\boldsymbol{\beta}) - \overline{L}(\boldsymbol{\beta}))^2 \tag{4.23}$$

where $\omega = 8.281 \times 10^{-3}$ mm^{-2} is the non-dimensionalizing factor, N denotes the total number of Gauss integration points in the product, L denotes the grain size (in mm) and the $\overline{(\cdot)}$ is used to represent the average grain size.

Fig. 15 shows the variation of the die shape during optimization iterations whereas Figs. 16 and 17 present the mean grain sizes in the intermediate preform (product after stage I) and the finished product. The variation of the objective function with the iteration index is shown in Fig. 18. Quantitatively speaking, the average grain size in the product obtained using the guess preforming die shape was observed to be around 64 μm with an average variation of about 40% of the initial grain size. In the product obtained using the optimal die shape, the average grain size was observed to be about 56 μm and the variation was seen to be less than 20% of the initial grain size.

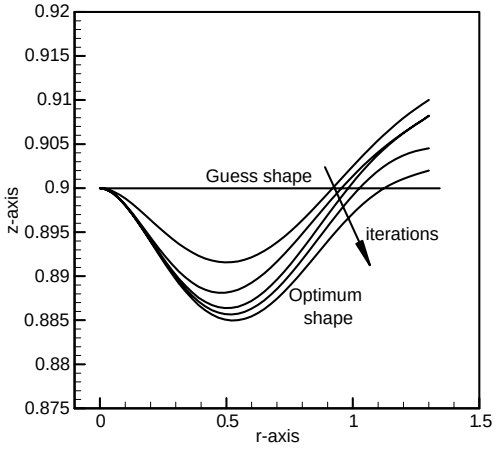

Fig. 15. The variation of the die shape with optimization iterations (Example 5).

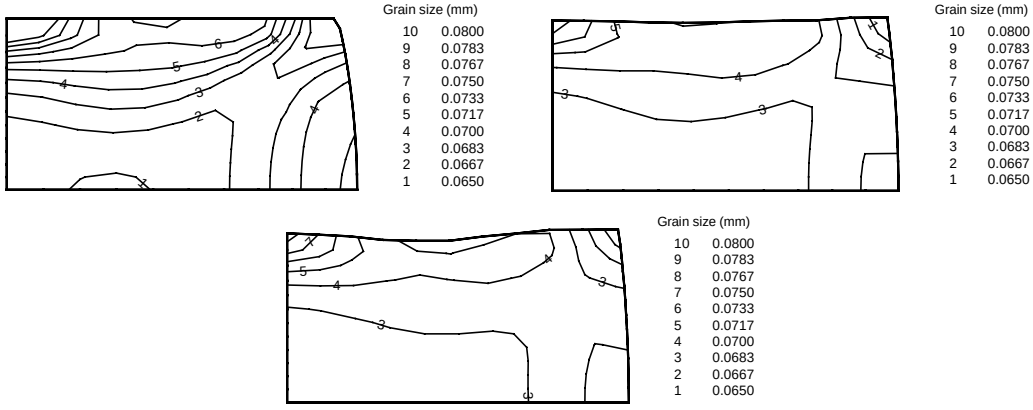

Fig. 16. Variation of the mean grain sizes and the intermediate preform using various die shapes during the optimization process (Example 5).

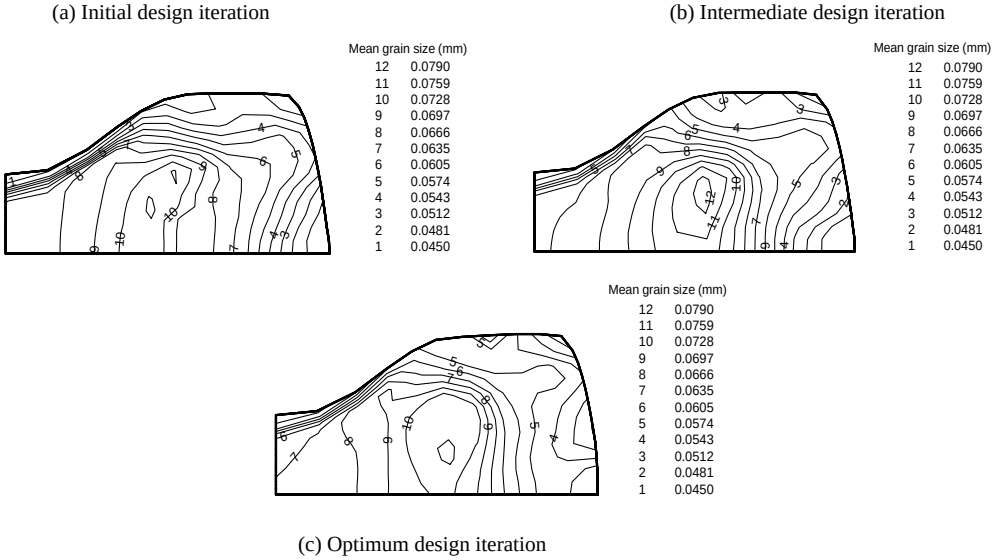

Fig. 17. Variation of the mean grain sizes in the final product using various die shapes at different stages of the optimization process (Example 5).

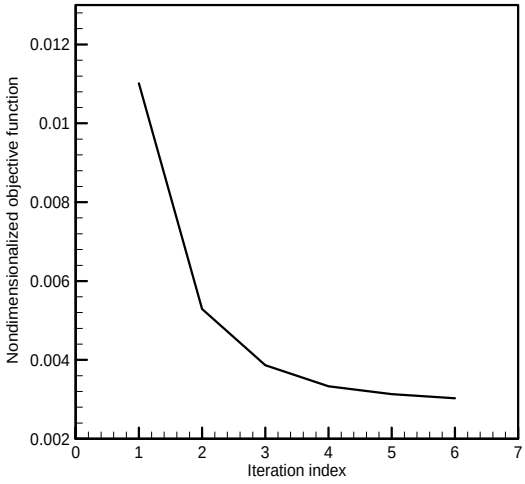

Fig. 18. The variation of the objective with iteration index (Example 5).

5. Discussion and conclusions

A hyperelastic, viscoplastic constitutive theory for large deformations has been proposed and implemented to describe the evolution of microstructural features at elevated temperatures. It involved descriptions of the kinetics of the grain size and the evolution of the dislocation resistance during dynamic recrystallization. As the current study deals only with dynamic recrystallization, the models used cannot predict the dynamics of static recrystallization. It is also observed that the onset of recrystallization is a

natural outcome of the evolution equations for the internal state variables, grain size L and the deformation resistance s. The volume fraction recrystallized is commonly defined by Eq. (4.7) and has been approximated to Eq. (4.8) in Busso (1998). Further, in Busso (1998), multiple peak recrystallization has also been analyzed by keeping track of the accumulated plastic strain since previous primary recrystallization. This is not valid since, the onset of recrystallization is no more an outcome of the state evolution equations alone. In this effort, multiple peak recrystallization is not considered even though it can be observed in many materials at low strain rates.

Furthermore, a novel and accurate continuum Lagrangian sensitivity framework was presented for non-isothermal, large deformations during metal forming processes. The CSM method was validated by comparing with the results obtained by a forward finite difference scheme. The computed sensitivities were used in a gradient-based optimization scheme to address a number of hot forming design examples including preform and die designs for industrial forming processes. Although, most aspects dealt with in this effort are phenomenological in nature, this work offers a first step and an attractive framework for future development of computational algorithms of process design for explicit control of the microstructure. Future efforts could incorporate static recrystallization, texture effects through the use of dislocation gradient concepts as well as anisotropy of grain boundary energies.

Acknowledgements

The work presented here was funded by the Computational Mathematics program of the Air Force Office of Scientific Research (grant F49620-00-1-0373) and by the National Science Foundation (grant DMI-0113295). Additional support was provided by the Materials Process Design Group of the Alcoa Technical Center (Dr. Paul Wang, program leader). This research was conducted using the resources of the Cornell Theory Center, which receives funding from Cornell University, New York State, federal agencies, and corporate partners.

References

Anand, L., 1985. Constitutive equations for hot-working of metals. International Journal of Plasticity 1, 213–231.

Badrinarayanan, S., Zabaras, N., 1996. A sensitivity analysis for the optimal design of metal forming processes. Computer Methods in Applied Mechanics and Engineering 129, 319–348.

Brown, S.B., Kim, K.H., Anand, L., 1989. An internal variable constitutive model for hot working of metals. International Journal of Plasticity 5, 95–130.

Busso, E.P., 1998. A continuum theory for dynamic recrystallization with microstructure related length scales. International Journal of Plasticity 14 (4–5), 319–351.

Cotterill, P., Mould, P.R., 1976. Recrystallization and Grain Growth in Metals. John Wiley and Sons, New York.

Dunne, F.P.E., Nanneh, M., Zhou, M., 1997. Anisothermal large deformation constitutive equations and their application to modelling titanium alloys in forging. Philosophical Magazine A 75 (3), 587–610.

Ganapathysubramanian, S., Zabaras, N., 2002. A continuum sensitivity method for finite thermo-inelastic deformations with applications to the design of hot forming processes. International Journal for Numerical Methods in Engineering 55, 1391–1437.

Ganapathysubramanian, S., Zabaras, N., 2003. Computational design of deformation processes for materials with ductile damage. Computer Methods in Applied Mechanics and Engineering 192, 147–183.

Gao, Z., Grandhi, R.V., 2000. Microstructure optimization in design of forging processes. International Journal of Machine Tools and Manufacture 40, 691–711.

Humphreys, F.J., Hatherly, M., 1995. Recrystallization and related annealing phenomena. Pergamon Press, New York.

Lee, S.K., Ko, D.C., Kim, B.M., 2000. Optimal die profile design for uniform microstructure in hot extruded product. International Journal of Machine Tools and Manufacture 40, 1457–1478.

Malas III, J.C., Frazier, W.G., Venugopal, S., Medina, E.A., Medeiros, S., Srinivasan, R., Irwin, R.D., Mullins, W.M., Chaudhary, A., 1997. Optimization of microstructure development during hot working using control theory. Metallurgical and Materials Transactions A 28, 1921–1930.

Nocedal, J., Wright, S.J., 1999. Numerical Optimization. Springer-Verlag, New York.

Srikanth, A., Zabaras, N., 1999a. A computational model for the finite element analysis of thermoplasticity coupled with ductile damage at finite strains. International Journal for Numerical Methods in Engineering 45, 1569–1605.

Srikanth, A., Zabaras, N., 1999b. Using objects to model finite deformation plasticity. Engineering With Computers 15, 37–60.

Srikanth, A., Zabaras, N., 2000. Shape optimization and preform design in metal forming processes. Computer Methods in Applied Mechanics and Engineering 190, 1859–1901.

Srikanth, A., Zabaras, N., 2001. An updated lagrangian finite element sensitivity analysis of large deformations using quadrilateral elements. International Journal for Numerical Methods in Engineering 52 (10), 1131–1163.

Weber, G., Anand, L., 1990. Finite deformation constitutive equations and a time integration procedure for isotropic, hyperelastic–viscoplastic solids. Computer Methods in Applied Mechanics and Engineering 79, 173–202.

Yada, H., Senuma, T., 1986. Resistance to hot deformation of steel. JJSTP 27, 34–44.

Zabaras, N., Srikanth, A., Yangang, B., Frazier, W.G., 2000. A continuum Lagrangian sensitivity analysis for metal forming processes with application to die design problems. International Journal for Numerical Methods in Engineering 48, 679–720.

Zabaras, N., Ganapathysubramanian, S., Li, Q., 2003. A continuum sensitivity method for the design of multi-stage metal forming processes. International Journal of Mechanical Sciences 45, 325–358.